American Journal of Biochemistry and Biotechnology

Original Research Paper

UPLC-QTOF-MS/MS and Bioinformatics Association Analysis Reveals the Pharmacodynamic Flavonoids in *Scutellaria barbata* and the Underlying Anti-Colorectal Cancer Mechanism

[1,2]Yi-Jie Cheng, [2]Xin-Yun Du, [1]Rui-Huan Chen, [2]Jing-Yuan Xu, [1]Ai-Guo Zhu, [2]Bo Jiang and [1]Xia Tian

[1]Department of Pharmacy, Changshu No.1 People's Hospital, Changshu Hospital Affiliated to Soochow University, Changshu, China
[2]School of Biology and Food Engineering, Changshu Institute of Technology, Changshu, China

Article history
Received: 22-06-2023
Revised: 26-08-2023
Accepted: 29-08-2023

Corresponding Author:
Xia Tian
Department of Pharmacy, Changshu No.1 People's Hospital, Changshu Hospital Affiliated to Soochow University, Changshu, China
Email: xctgbz666@163.com

Abstract: Colorectal Cancer (CRC) is one of the most common and deadly malignancies worldwide, with no safe and effective drugs. The flavonoid in *Scutellaria Barbata* D. Don (SB) showed a good therapeutic effect on CRC. However, the pharmacodynamic substances and underlying mechanisms have not been elucidated which limited its development and application. This study aimed to identify the main flavonoid in SB and explore the underlying mechanism. A total of 10 flavonoid aglycones identified by UPLC-QTOF-MS/MS were screened out as candidate compounds with good drug-likeness. By using the predicted targets of candidate compounds for CRC treatment, KEGG pathway analysis enriched 5 CRC-related pathways. Further analysis revealed that targets mapped to the five selected pathways were mainly correlated to the PI3K-Akt signaling pathway. The key targets were AKT1, VEGFA, EGFR, SRC, and MTOR. Molecular docking combined with the RNA sequencing analysis on CRC patients validated the high potential binding ability of candidate compounds to differentially expressed targets in the PI3K-Akt signaling pathway. Collectively, this study revealed that the flavonoid aglycones in SB may be the key ingredients contributing to its CRC treatment function and they exerted the CRC treatment effect by synergistic effect of multiple targets mainly belonging to the PI3K-Akt signaling pathway.

Keywords: Colorectal Cancer, *Scutellaria barbata*, UPLC-QTOF-MS/MS, Bioinformatics Analysis, PI3K-Akt Signaling Pathway

Introduction

Colorectal Cancer (CRC) is a prevalent malignant tumor of the digestive tract, with an estimated annual incidence of over 1.85 million new cases worldwide and it has now become the second most common cause of cancer-related deaths globally (Biller and Schrag, 2021; Sawicki *et al*., 2021). It is still a challenge for effective clinical treatment of patients with CRC. In recent years, CRC incidence in China has also continued to increase, which has become an important issue affecting public health (Zheng *et al*., 2022). Currently, the treatment strategy for CRC entails a multimodal approach, which includes surgical resection as well as comprehensive therapies such as chemotherapy, radiotherapy, targeted therapy, and immunotherapy. The related drugs mainly include active cytotoxic drugs such as irinotecan, oxaliplatin, 5-fluorouracil, and capecitabine, as well as biological agents including bevacizumab, cetuximab and panitumumab (Cartwright, 2012). However, conventional chemotherapeutic treatments have many side effects and are especially likely to develop drug resistance. In comparison to the standard treatment, targeted therapy and immunotherapy are new alternative options but require patients to bear high medical costs (Dekker *et al*., 2019). Thus, it is crucial to develop more cost-effective and less toxic drugs against CRC.

Due to its favorable efficacy and minimal toxicity, Traditional Chinese Medicine (TCM) has gained increasing recognition in the treatment of CRC. Many traditional Chinese medicines, such as Si-Jun-Zi Decoction and Xiao-Ai-Jie-Du Decoction, have shown great potential *in vivo* and *in vitro* for the treatment of

CRC (Fan *et al*., 2020; Shang *et al*., 2023). *Scutellariae barbata* herba (Ban-Zhi-Lian in Chinese) is the dried full plant of *Scutellaria Barbata* D. Don (SB) in the Lamiaceae family, which has been commonly used as heat-clearing and detoxifying herbal medicine for thousands of years (Wang *et al*., 2020a). It has also been used for the treatment of CRC as a single herb or component in TCM formulae (Chen *et al*., 2018a; Fan *et al*., 2020; Lin *et al*., 2017a). In addition, it was confirmed that the extracts of SB exhibited good anti-CRC activity *in vivo* and *in vitro*. It was discovered that the aqueous extract of SB demonstrated inhibitory effects on the growth and metastasis of CRC in a mouse model with HCT116 transplanted tumors (Yue *et al*., 2021). Wei *et al*. (2013) reported that the ethanol extract of SB could also suppress the proliferation of HT-29 cells. Therefore, SB deserves to do further research for the development of new drugs against CRC.

Secondary metabolites are the material basis for the efficacy of TCM. Pharmacological research verified flavonoids were the important active components against CRC in SB. Liu *et al*. (2022a) reported flavonoids in SB showed significant antitumor activity in CRC by inhibiting autophagy and promoting apoptosis. Li *et al*. (2020) found that scutellarein, a main flavonoid identified in SB, could induce apoptosis of colon cancer SW480 cells by upregulating CDC4-mediated RAGE ubiquitination. However, due to the variety of flavonoids in SB, the definite pharmacodynamic ingredients and related anti-CRC mechanisms have not been sufficiently defined.

As systems biology and bioinformatics developed rapidly, Network Pharmacology (NP) has developed into a viable tool to understand the complex mechanisms of TCM. It can promote the transformation of TCM research from the traditional single-drug, single-target model to a synergistic model which is more in line with the holistic characteristic of TCM (Li *et al*., 2022; Yuan *et al*., 2017). The UPLC-HRMS provides a favorable means for broad-spectrum identification of chemical constituents in TCM. Researchers have tried to combine UPLC-HRMS and NP to screen active ingredients and better understand the complex mechanisms of TCM (Bi *et al*., 2021).

Therefore, the NP and UPLC-HRMS were combined to explore the active flavonoids against CRC in SB and elucidate their underlying mechanism of CRC treatment. In addition, the targets of SB flavonoids against CRC were verified by using human transcriptomic data and molecular docking.

This study provides a reference for elucidating the anti-colorectal mechanisms of SB and further developing anti-CRC drugs based on SB. Figure 1 is the overview of a flow diagram.

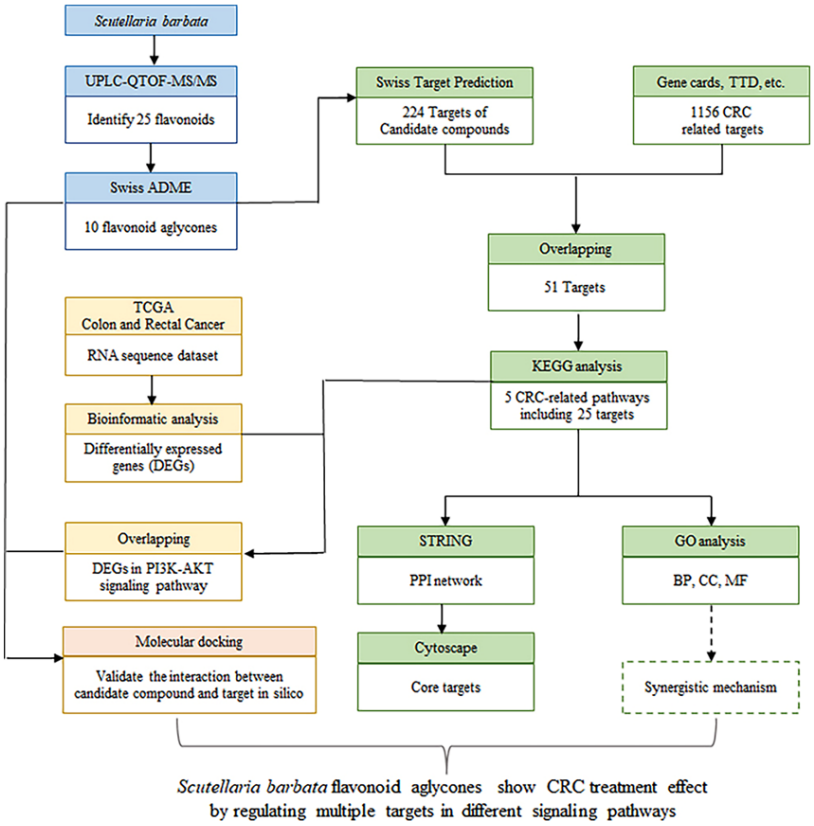

Fig. 1: Overall design of this study

Materials and Methods

Qualitative Analysis Based on UHPLC-QTOF-MS/MS

SB was collected from the botanic garden of Changshu Institute of Technology (May 2021; Changshu, China) and identified by Professor Bo Jiang. The voucher was deposited in herbarium (No. SB20210501). The dried samples were crushed and the 50 mg power was accurately weighed. Then the sample was extracted according to the reference (Xu *et al*., 2018).

Qualitative Analysis was performed on UPLC-HRMS in negative ion modes according to our previous report with slight modifications (Cheng *et al*., 2022). The gradient duration program is shown in Table 1.

The ADME Evaluation and Targets Collection of Identified Flavonoids

The ADME parameters of the identified flavonoid in SB were calculated by the SwissADME online tool (http://www.swissadme.ch (accessed on 15 November 2022)) (Daina *et al*., 2017). The identified flavonoid which met the requirement of Lipinski's rule of five was screened out as a candidate compound (Zeng *et al*., 2021). After that, the SwissTargetPrediction online tool (http://www.swisstargetprediction.ch/index.php (accessed on 22 November 2022)) was used to predict the potential targets of candidate compounds (Daina *et al*., 2019).

Screening Targets of Candidate Compounds Against CRC

The disease targets related to CRC were gathered from the open source database which includes GeneCards database (https://www.genecards.org/(accessed on 30 November 2022)), DisGenet database (https://www.disgenet.org/home/(accessed on 30 November 2022)), OMIM database (https://omim.org/(accessed on 30 November 2022)) and TTD database (https://db.idrblab.net/ttd/ (accessed on 30 November 2022)). Then, the common targets of candidate compounds and CRC were screened out by an online tool (https://bioinfogp.cnb.csic.es/tools/venny/index.html). The overlapped targets were the potential targets of candidate compounds against CRC.

KEGG and GO Enrichment Analysis

The KEGG pathway enrichment analysis was performed by Metascape (https://metascape.org/gp/index.html#/main/step1 (accessed on 2 December 2022)) (Zhou *et al*., 2019). The top 20 enriched KEGG pathways were visualized and the CRC-related pathways were selected. On this basis, the targets belonging to the selected pathways were further performed GO enrichment analysis. The GO enrichment was conducted by Metascape with the same enrichment parameters as above described.

Protein-Protein Interaction (PPI) Analysis

The PPI network was constructed by using the String online tool (https://cn.string-db.org/ (accessed on 3 December 2022)) (Szklarczyk *et al*., 2019). The result was further analyzed by Network Analyzer which was a plugin of Cytoscape (version 3.7.2). The top 10 targets ranked by degree values in the PPI network were identified as core targets (Zeng *et al*., 2021).

Identification of CRC Differentially Expressed Genes (DEGs)

The gene expression RNA sequencing data and clinical information on 434 CRC patients (dataset ID: TCGA.COADREAD.sampleMap/HiSeqV2) were derived from the cohort of 'TCGA Colon and Rectal Cancer' in the UCSC cancer browser (https://tcga.xenahubs.net (accessed on 15 December 2022)) (Zhang *et al*., 2021). The RNA sequencing data was collected from 434 CRC patients including 383 tumor samples and 51 normal tissue samples. The data was first processed by principal component analysis to omit the samples that were not included in the first two principal components. Then DEG analysis was conducted through the R software Limma package (version 3.40.6). The genes with fold change >1.5 and $p<0.01$ were defined as DEGs.

Molecular Docking

To further validate the binding ability of candidate compounds to potential targets, molecular docking was carried out using the auto dock tools (version 1.5.6). The protein structures of targets were retrieved from the RCSB protein data bank (https://www.rcsb.org/). The selected protein structure should meet the following criteria: (1) The protein was without mutation, (2) The resolution must be higher than 2.5Å and (3) There should be an inhibitor in the protein. The protein was pre-processed by PyMOL (version 4.6) to remove heteroatom. After that, the candidate compound was docked to the active sites of the target by auto dock tools. The position of the original ligand of the protein as the center of the docking box and the size of the grid box is set to 40*40*40 (with a spacing of 0.375 Å between each grid point). During the docking process, the number of GA runs is set to 100, while the rest of the docking parameters are set as 'user defaults'. The interaction between ligand and receptor was visualized by PyMOL.

Table 1: The chromatographic elution program

Timepoint (min)	Water with 0.1% formic acid (A %)	Acetonitrile (B %)
0	90	10
10	84	16
18	70	30
21	5	95
23	5	95

Results

Qualitative Analysis of SB

To better explain and identify the ingredients in SB, UHPLC-QTOF-MS/MS was applied in our study for qualitative analysis. The base peak chromatogram in the negative ion model is shown in Fig. 2A. The element compositions of the compound and its MS^2 fragment ions can be calculated by their accurate mass measurements. Further compared with the published literature and database, the ingredients would be identified. In negative anion mode, the loss of glycosyl is a character of flavonoid glycoside. After that, the fragment ion might further lose neutral fragments. Compound 6 showed $[M-H]^-$ion at m/z 461.0734 ($C_{21}H_{17}O_{12}$). The MS^2 spectrum showed fragment ion $[M-H-176]^-$ at 285.0429 ($C_{15}H_9O_6$) indicating a glucuronic acid residue in compound 6. The fragment ion at 267.0536 ($C_{15}H_7O_5$) was due to the loss of an H_2O from fragment ion 285.0429 $[M-H-C_6H_8O_6]^-$. The fragment ion at 239.0365 ($C_{14}H_7O_4$) was due to the loss of a CO from fragment ion 267.0536 $[M-H-C_6H_8O_6-H_2O]^-$. Compared with published data (Kang *et al*., 2022), it was identified as scutellarin shown in Fig. 2B. The $X^{1,3}$ cleavage of C-ring in flavonoid aglycones is another characteristic of flavonoids (Li *et al*., 2015). It produced the main fragment ions $^{1,3}A$ and $^{1,3}B$ in the MS^2 spectrum. Compound 17 showed $[M-H]^-$ion at m/z 285.0423 ($C_{15}H_9O_6$). The quasi-molecular ion generated fragment ions at m/z 151.0046 $[C_7H_3O_4]^-$ and 133.0280 $[C_8H_5O_2]^-$ through the $X^{1,3}$ cleavage of C-ring. Compared with the literature (Kang *et al*., 2022), this compound was speculated as luteolion shown in Fig. 2C. The other compounds were identified in the same way. In this way, 27 different compounds were identified including 25 flavonoid compounds (Table 2). The structures of the identified compounds are shown in Fig. S1 It can be concluded that flavonoid was the main component in SB.

The ADME Proprieties of the Identified Flavonoid Compounds in SB

Early estimation of ADME is important for screening active ingredients to reduce drastically the pharmacokinetics-related failure in the clinical phases (Hay *et al*., 2014). In this study, an online swissADME tool was used to evaluate the ADME proprieties of the identified flavonoid in SB shown in Table 2. As shown in Table 3, 10 compounds in line with Lipinski' rule of five were screened from the 25 identified flavonoids which were scutellarein (molecule13), luteolin (molecule15), 6-methoxyluteolin (Molecule16), 8-methoxyluteolin (molecule17), naringenin (molecule18), 6-methoxynaringenin (molecule19), 5,7,4'-trihydroxy-8-methoxyflavanone (molecule20), apigenin (molecule21), 4'-hydroxywogonin (molecule22) and hispidulin (molecule23). The structures of screened compounds are shown in Fig. 3. These screened compounds were all belonged to flavonoid aglycone and used as candidate compounds for subsequent analysis. These results indicated that the flavonoid aglycones in SB owned better pharmacokinetic proprieties, which might be the key ingredients against CRC in SB.

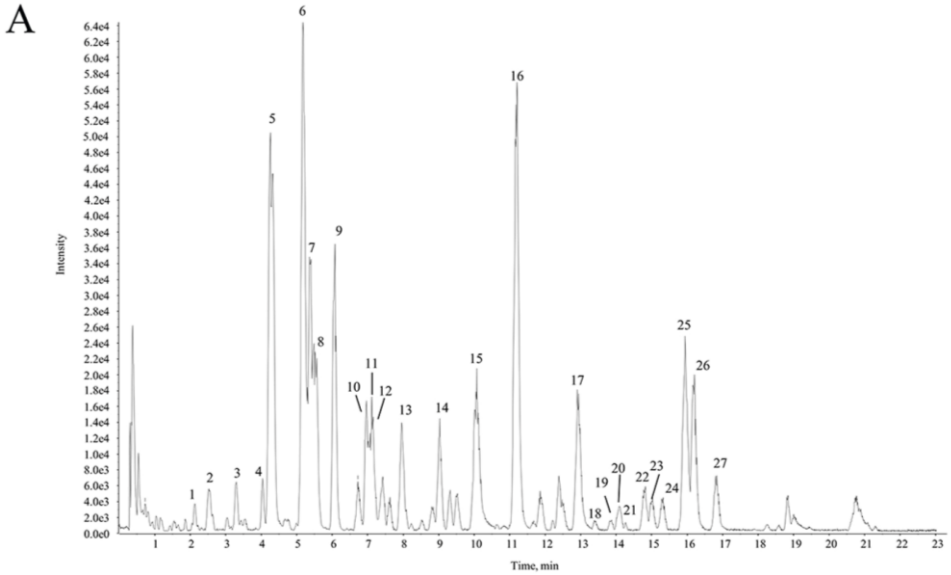

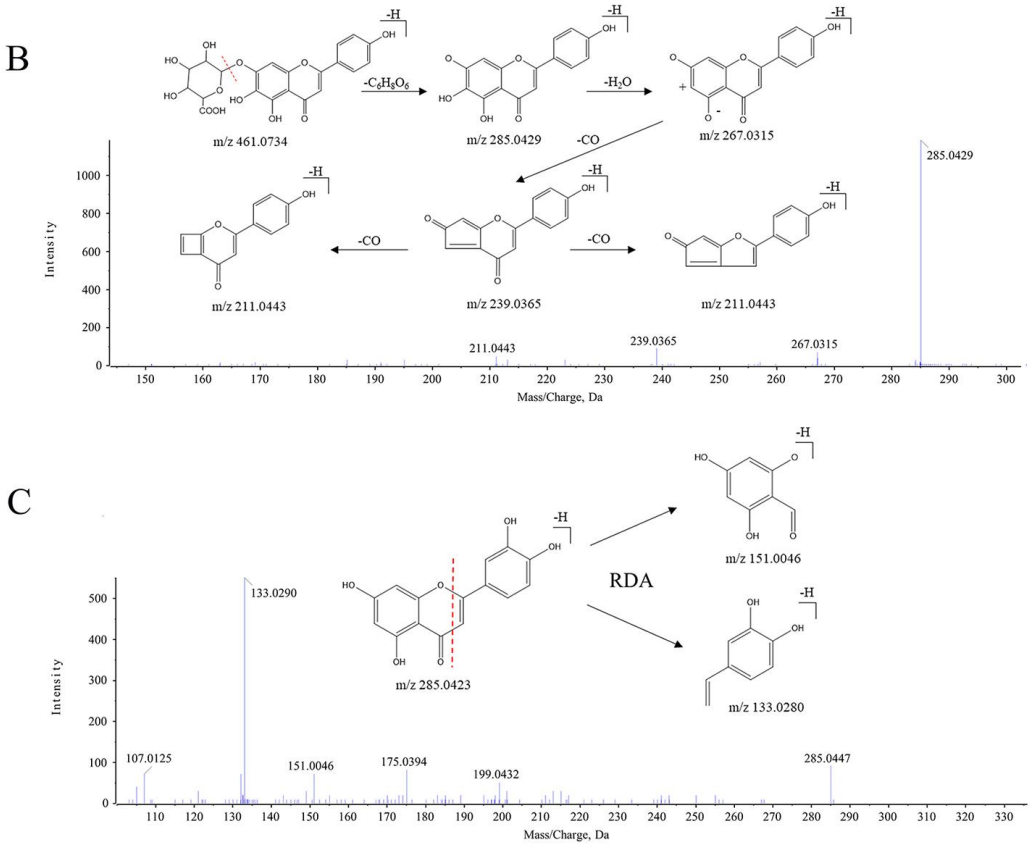

Fig. 2: Base peak chromatogram of SB in negative mode and the ESI¬MS/MS spectra of typical flavonoid; (A) Base peak chromatogram of SB; (B) MS/MS spectra and speculated cleavage mode of scutellarin; (C) MS/MS spectra and speculated cleavage mode of lute

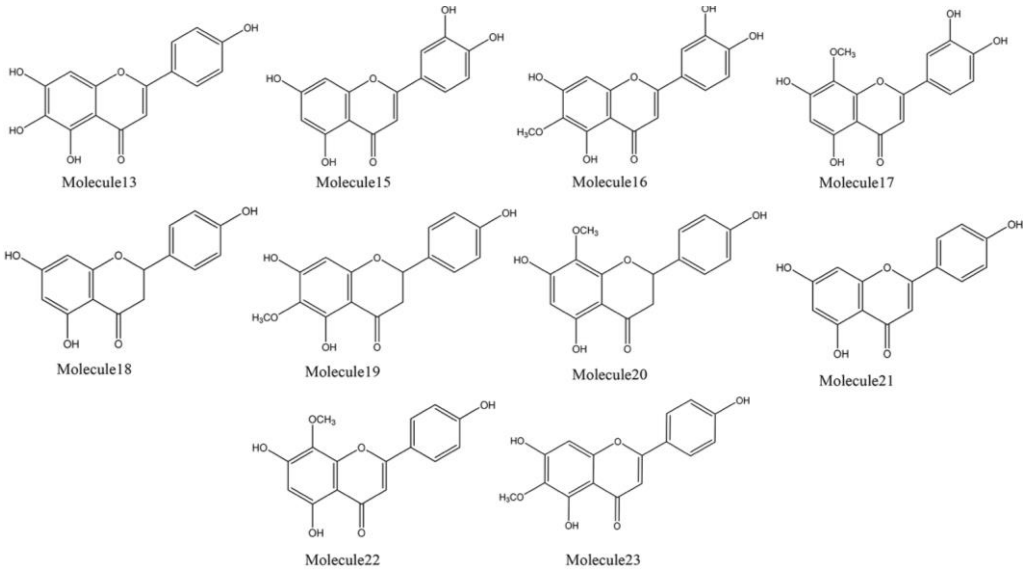

Fig. 3: Structures of the screened flavonoids in SB. Molecule13: Scutellarein, molecule15: Luteolin, molecule16: 6-methoxyluteolin, molecule17: 8-methoxyluteolin, molecule18: Naringenin, molecule19: 6-methoxynaringenin, molecule20: 5,7,4'-trihydroxy-8-meth

Table 2: Identified compounds in SB

Peak no.	RT	Name	Molecular formula	Measured $[M-H]^-$	Predicted $[M-H]^-$	Error (ppm)	MS/MS fragments ions
1	2.14	Luteolin-7-O-rutinoside (Zhang *et al*., 2015)	$C_{27}H_{30}O_{15}$	593.1526	593.1512	2.4	503.1319, 473.1191, 383.0841, 353.0723
2	2.53	Dihydroviscidulin I-7-O-glucuronide (Zhang *et al*., 2015)	$C_{21}H_{20}O_{13}$	479.0845	479.0831	2.9	303.0607, 285.0557, 181.0201, 167.0041, 153.0214, 139.0066, 135.0477
3	3.28	6-Hydroxyluteolin-7-O- glucuronide (Li *et al*., 2015)	$C_{21}H_{18}O_{13}$	477.0684	477.0675	2.0	301.0438, 283.0310, 255.0327
4	4.062	Luteoline -7-O-glucoside (Li *et al*., 2015)	$C_{21}H_{20}O_{11}$	447.0945	447.0933	2.7	285.0428, 217.0484, 151.0019
5	4.26	Isocarthamidin-7-O-glucuronide (Zhang *et al*., 2015)	$C_{21}H_{20}O_{12}$	463.0890	463.0882	1.7	287.0597, 269.0474, 259.0635, 193.0131, 181.0140, 166.9982, 153.0187, 139.0024, 119.0493
6	5.184	Scutellarin (Kang *et al*., 2022)	$C_{21}H_{18}O_{12}$	461.0734	461.0725	1.8	285.0429, 267.0315, 239.0365, 211.0443
7	5.358	Isomer of scutellarin	$C_{21}H_{18}O_{12}$	461.0748	461.0725	4.9	286.0742, 241.0513, 133.0297
8	5.58	Carthamidin-7-O-glucuronide (Zhang *et al*., 2015)	$C_{21}H_{20}O_{12}$	463.0895	463.0882	2.8	287.0578, 269.0460, 259.0650, 193.0131, 181.0130, 166.9970, 153.0180, 139.0020, 119.0490
9	6.073	Apigenin-7-O-glucoside (Zhang *et al*., 2015)	$C_{21}H_{20}O_{10}$	431.0998	431.0984	3.3	269.0481, 225.0570, 183.0450, 149.0224, 117.0326
10	6.963	Acteoside (Li *et al*., 2015)	$C_{29}H_{36}O_{15}$	623.2011	623.1981	4.7	623.2197, 461.1812, 315.1133, 161.0267
11	7.123	Scutellarein -7-O-glucoside (Li *et al*., 2015)	$C_{21}H_{20}O_{11}$	447.0955	447.0933	5.0	285.0473, 267.0290, 255.0278, 239.0376, 227.038
12	7.136	Luteolin-7-O-glucuronide (Zhang *et al*., 2015)	$C_{21}H_{18}O_{12}$	461.0753	461.0725	6.0	285.0482, 267.0392, 239.0412, 211.0428
13	7.919	Apigenin-7-O-glucuronide (Li *et al*., 2016)	$C_{21}H_{18}O_{11}$	445.0793	445.0776	3.7	269.0536, 225.0571, 117.0212
14	9.035	4'-Hydroxywogonin-7-O-glucuronide (Li *et al*., 2015)	$C_{22}H_{20}O_{12}$	475.0905	475.0882	4.8	284.0415, 214.0298, 163.0074, 117.0186
15	10.064	Scutellarein (Kang *et al*., 2022)	$C_{15}H_{10}O_6$	285.0406	285.0405	0.5	257.0569, 239.0393, 195.0470,137.0221, 119.0514, 117.0335
16	11.19	Isoscutellarein 8-O-glucuronide (Li *et al*., 2015)	$C_{21}H_{18}O_{12}$	461.074	461.0725	3.1	285.0443, 257.0476, 241.0552, 229.0523, 213.0576, 187.0401, 185.0579, 145.0292,
17	12.927	Luteolin (Kang *et al*., 2022)	$C_{15}H_{10}O_6$	285.0423	285.0405	2.9	241.0547, 199.0432, 175.0394, 151.0046, 133.0280, 107.0125
18	13.405	6-Methoxyluteolin (Kang *et al*., 2022)	$C_{16}H_{12}O_7$	315.0505	315.0510	-1.7	300.0315, 299.0157, 243.0334, 136.9901, 133.0274
19	13.832	8-Methoxyluteolin (Kang *et al*., 2022)	$C_{16}H_{12}O_7$	315.0523	315.0510	4.0	300.0343, 243.0303, 136.857, 133.0265
20	14.093	Isomer of 6-Methoxynaringenin (Kang *et al*., 2022)	$C_{16}H_{14}O_6$	301.0731	301.0718	4.4	180.0056, 165.9894, 137.9921, 119.0476, 109.9988
21	14.255	Cistanoside D (Li *et al*., 2015)	$C_{31}H_{40}O_{15}$	651.2351	651.2294	8.7	475.182, 193.0505, 175.0396, 160.0149
22	14.796	Naringenin (Kang *et al*., 2022)	$C_{15}H_{12}O_5$	271.0614	271.0612	0.7	151.0052, 119.0488, 107.0133
23	15.015	6-Methoxynaringenin	$C_{16}H_{14}O_6$	301.0729	301.0718	3.8	286.0447, 185.0587,

Table 2: Continue

		(Zhang *et al*., 2015)					180.0027, 165.9896, 119.0507, 109.9988
24	15.33	5,7,4'-Trihydroxy-8-methoxyflavanone (Zhang *et al*., 2015)	$C_{16}H_{14}O_6$	301.0729	301.0718	-2.5	286.0531, 165.9889, 137.9935, 119.0470, 109.9992
25	15.952	Apigenin (Kang *et al*., 2022)	$C_{15}H_{10}O_5$	269.0455	269.0455	-0.2	227.0283, 183.0437, 159.0428, 151.0007, 117.0332, 107.0145
26	16.181	4'-Hydroxywogonin (Kang *et al*., 2022)	$C_{16}H_{12}O_6$	299.0566	299.0561	1.6	284.0351, 255.0346, 227.0360, 183.0454, 136.9867, 117.0326
27	16.773	Hispidulin (Kang *et al*., 2022)	$C_{16}H_{12}O_6$	299.0565	299.0561	1.3	284.0379, 255.0418, 227.0397, 183.0474, 158.0435, 136.9873

Table 3: Pharmacological and molecular properties of the indentified flavonoids in SB

Molecule	Name	Formula	MW(g/mol)	Hdon	Hacc	Rbon	TPSA	LogP	Logs
1	Luteolin-O-rutinoside	$C_{26}H_{28}O_{16}$	596.49	10	16	6	269.43	-1.65	-3.29
2	Dihydroviscidulin I-7-O-glucuronide	$C_{21}H_{20}O_{13}$	480.38	8	13	4	223.67	-1.08	-2.77
3	6-Hydroxyluteolin-7-O-glucuronide	$C_{21}H_{20}O_{12}$	464.38	8	12	4	210.51	-0.1	-3.14
4	Luteoline -7-O-glucoside	$C_{21}H_{20}O_{11}$	448.38	7	11	4	190.28	0.15	-3.65
5	Isocarthamidin-7-O-glucuronide	$C_{21}H_{20}O_{12}$	464.38	7	12	4	203.44	-0.41	-3.03
6	Scutellarin	$C_{21}H_{18}O_{12}$	462.36	7	12	4	207.35	-0.22	-3.27
7	Carthamidin-7-O-glucuronide	$C_{21}H_{20}O_{12}$	464.38	7	12	4	203.44	-0.38	-3.03
8	Apigenin-7-O-glucoside	$C_{21}H_{20}O_{10}$	432.38	6	10	4	170.05	0.52	-3.78
9	Scutellarein-7-O-glucoside	$C_{21}H_{20}O_{11}$	448.38	7	11	4	190.28	-0.07	-3.05
10	Luteolin-7-O-glucuronide	$C_{21}H_{18}O_{12}$	462.36	7	12	4	207.35	-0.06	-3.41
11	Apigenin-7-O-glucuronide	$C_{21}H_{18}O_{11}$	446.36	6	11	4	187.12	0.29	-3.63
12	4'-Hydroxywogonin-7-O-glucuronide	$C_{22}H_{20}O_{12}$	476.39	6	12	5	196.35	0.27	-3.49
13	Scutellarein	$C_{15}H_{10}O_6$	286.24	4	6	1	111.13	1.81	-3.79
14	Isoscutellarein 8-O-glucuronide	$C_{23}H_{22}O_{11}$	474.41	6	11	5	183.21	0.57	-3.27
15	Luteolin	$C_{15}H_{10}O_6$	286.24	4	6	1	111.13	1.73	-3.71
16	6-Methoxyluteolin	$C_{16}H_{12}O_7$	316.26	4	7	2	120.36	1.74	-3.76
17	8-Methoxyluteolin	$C_{16}H_{12}O_7$	316.26	4	7	2	120.36	1.74	-3.76
18	Naringenin	$C_{15}H_{12}O_5$	272.25	3	5	1	86.99	1.84	-3.49
19	6-Methoxynaringenin	$C_{16}H_{14}O_6$	302.28	3	6	2	96.22	1.86	-3.55
20	5,7,4'-Trihydroxy-8-methoxyflavanone	$C_{15}H_{12}O_5$	272.25	3	5	1	86.99	1.84	-3.55
21	Apigenin	$C_{15}H_{10}O_5$	270.24	3	5	1	90.90	2.11	-3.94
22	4'-Hydroxywogonin	$C_{16}H_{12}O_6$	300.26	3	6	2	100.13	2.12	-3.99
23	Hispidulin	$C_{16}H_{12}O_6$	300.26	3	6	2	100.13	2.12	-3.99

MW: Molecule Weight; Hdon: Hydrogen bond donors; Hacc: Hydrogen bond acceptors; Rbon: Rotatable bonds; TPSA: Topological Polar Surface Area; LogP: Lipid-water partition coefficient; LogS: Solubility

Targets of Candidate Compounds Against CRC

In total, 224 potential targets were obtained based on the structure of candidate compounds, and 1156 CRC-related targets were collected from public databases. Ultimately, there were 51 potential targets of candidate compounds against CRC screened out by overlapping the candidate compounds targets and the CRC-related targets (Fig. 4). In addition, among the screened CRC disease targets, 1105 predicted targets were not matched with the candidate compounds targets. Detailed information on the selected targets is shown in Table 4.

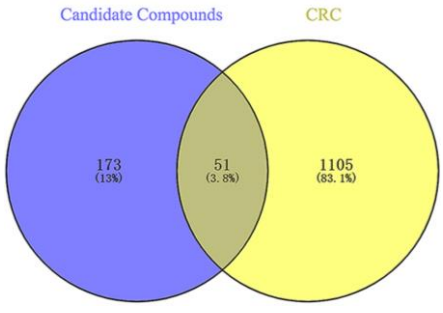

Fig. 4: Potential targets of the candidate compounds against CRC. The overlaps meant the potential targets of the screened compounds against CRC

Table 4: Targets of the candidate compounds in SB against CRC

No.	Uniprot ID	Gene symbol	Description
1	Q13332	PTPRS	Receptor-type tyrosine-protein phosphatase S
2	P33527	ABCC1	Multidrug resistance-associated protein 1
3	Q16678	CYP1B1	Cytochrome P450 1B1
4	Q9UNQ0	ABCG2	ATP-binding cassette sub-family G member 2
5	P03372	ESR1	Estrogen receptor alpha
6	Q92731	ESR2	Estrogen receptor beta
7	P30542	ADORA1	Adenosine A1 receptor
8	O60218	AKR1B10	Aldo-keto reductase family 1 member B10
9	P08183	ABCB1	P-glycoprotein 1
10	O14746	TERT	Telomerase reverse transcriptase
11	P09874	PARP1	Poly [ADP-ribose] polymerase-1
12	P14780	MMP9	Matrix metalloproteinase 9
13	P08253	MMP2	Matrix metalloproteinase 2
14	P11387	TOP1	DNA topoisomerase I (by homology)
15	P35354	PTGS2	Cyclooxygenase-2 (by homology)
16	P13569	CFTR	Cystic fibrosis transmembrane conductance regulator
17	P10275	AR	Androgen Receptor
18	P08069	IGF1R	Insulin-like growth factor I receptor
19	P00533	EGFR	Epidermal growth factor receptor erbB1
20	P05164	MPO	Myeloperoxidase
21	P27986	PIK3R1	PI3-kinase p85-alpha subunit
22	P12931	SRC	Tyrosine-protein kinase SRC
23	P35968	KDR	Vascular endothelial growth factor receptor 2
24	P08581	MET	Hepatocyte growth factor receptor
25	Q9UM73	ALK	ALK tyrosine kinase receptor
26	P31749	AKT1	Serine/threonine-protein kinase AKT
27	P10721	KIT	Stem cell growth factor receptor
28	P14555	PLA2G2A	Phospholipase A2 group IIA
29	P04798	CYP1A1	Cytochrome P450 1A1
30	P05177	CYP1A2	Cytochrome P450 1A2
31	P48736	PIK3CG	PI3-kinase p110-gamma subunit
32	P11926	ODC1	Ornithine decarboxylase
33	P37231	PPARG	Peroxisome proliferator-activated receptor gamma
34	P11362	FGFR1	Fibroblast growth factor receptor 1
35	P16083	NQO2	Quinone reductase 2
36	P17936	IGFBP3	Insulin-like growth factor binding protein 3
37	Q07817	BCL2L1	Apoptosis regulator Bcl-X
38	P42338	PIK3CB	PI3-kinase p110-beta subunit
39	P42336	PIK3CA	PI3-kinase p110-alpha subunit
40	P15692	VEGFA	Vascular endothelial growth factor A
41	P10415	BCL2	Apoptosis regulator Bcl-2
42	P11802	CDK4	Cyclin-dependent kinase 4
43	O14965	AURKA	Serine/threonine-protein kinase Aurora-A
44	P26358	DNMT1	DNA (cytosine-5)-methyltransferase 1
45	Q9NR96	TLR9	Toll-like receptor (TLR7/TLR9)
46	P23443	RPS6KB1	Ribosomal protein S6 kinase 1
47	O60674	JAK2	Tyrosine-protein kinase JAK2
48	P21980	TGM2	Protein-glutamine gamma-glutamyltransferase
49	P15559	NQO1	Quinone reductase 1
50	P15056	BRAF	Serine/threonine-protein kinase B-raf
51	P42345	MTOR	Serine/threonine-protein kinase mTOR

KEGG Pathway Analysis and GO Functional Enrichment Analysis

The KEGG enrichment analysis was performed by the Metascape online tool to systematically discern the signal pathways associated with 51 potential targets of candidate compounds against CRC. It obtained 135 KEGG pathway items with p cut-off value <0.01 (Raw data is available upon request from the corresponding author) and the top 20 enriched signaling pathways were visualized based on p-value (Fig. 5). The detailed information on the top 20 signal pathways was shown in Table 5. There were 5 CRC-related signaling pathways screened out from the top 20 enriched signaling

pathways which were EGFR tyrosine kinase inhibitor resistance, PI3K-Akt signaling pathway, Rap1 signaling pathway, Ras signaling pathway, and Estrogen signaling pathway. The above results demonstrated that the candidate compounds could exert CRC against efficacy through multiple signal pathways.

GO enrichment analysis is commonly used to comprehensively describe the attributes of genes and gene products from three different levels, including Molecular Function (MF), Biological Process (BP), and Component analysis (CC). BP analysis mainly describes the biological processes in which genes are involved, aiding researchers in understanding the physiological functions and mechanisms of disease occurrence in the organism. MF analysis is used to understand the molecular-level functions of gene products, often involving interactions with other molecules or catalyzing biochemical reactions. CC analysis can show the cellular localization of gene products (e.g., proteins), helping to understand their roles and functions within the cell. Therefore, Targets in the five selected CRC-related signaling pathways were further performed GO enrichment analysis. In this study, a total of 652 BP items, 42 MF items, and 25 CC items were enriched (Raw data is available upon request from the corresponding author). The top 10 items of BP, CC, and MF with smaller p-values in GO enrichment analysis are shown in Fig. 6. The results demonstrated that the candidate compounds exhibited anti-CRC effects through various BPs. These processes predominantly involve positive regulation of cell migration and motility, as well as the modulation of signaling pathways such as transmembrane receptor protein tyrosine kinase, enzyme-linked receptor protein, protein phosphorylation, and hormone response. The related targets could be classified into different cellular components such as receptor complex, transferase complex, transferring phosphorus-containing groups, cell-cell junction, perinuclear region of cytoplasm, and mitochondrial membrane. These targets showed multiple molecular functions including phosphotransferase activity, alcohol group as acceptor, protein serine kinase activity, protein serine/threonine kinase activity, transmembrane receptor protein tyrosine kinase activity, and protein kinase binding activity.

PPI Network Construction

To explore the relationship of targets in selected CRC-related signaling pathways, the STRING online platform was used to construct a protein-protein interaction network that contained 25 nodes and 386 edges. The average node degree was 15.4. The degree represented the number of target interactions. The targets with a larger degree might interact with other targets. As shown in Fig. 7, the nodes with darker colors owned a greater degree. The five core targets with higher degrees, namely AKT1, VEGFA, EGFR, SRC, and MTOR, were likely to be closely interrelated with other targets in the PPI network. They might also have significant regulatory effects on candidate compounds for CRC treatment.

Table 5: Top 20 KEGG pathway terms enriched by the targets of candidate compounds against CRC

Term	Pathway	Enrichment	p-value	Count	Symbols
hsa05200	Pathways in cancer	30.079	3.420×10^{-34}	27	AKT1, ALK, AR, BCL2, BCL2L1, BRAF, CDK4, NQO1, EGFR, ESR1, ESR2, FGFR1, MTOR, IGF1R, JAK2, KIT, MET, MMP2, MMP9, PIK3CA, PIK3CB, PIK3R1, PPARG, PTGS2, RPS6KB1, TERT, VEGFA
hsa01521	EGFR tyrosine kinase inhibitor resistance	119.807	6.442×10^{-30}	16	AKT1, BCL2, BCL2L1, BRAF, EGFR, MTOR, IGF1R, JAK2, KDR, MET, PIK3CA, PIK3CB, PIK3R1, RPS6KB1, SRC, VEGFA
hsa01522	Endocrine resistance	96.579	2.77×10^{-28}	16	AKT1, BCL2, BRAF, CDK4, EGFR, ESR1, ESR2, MTOR, IGF1R, MMP2, MMP9, PIK3CA, PIK3CB, PIK3R1, RPS6KB1, SRC
hsa05205	Proteoglycans in cancer	49.055	8.165×10^{-25}	17	AKT1, BRAF, EGFR, ESR1, FGFR1, MTOR, IGF1R, KDR, MET, MMP2, MMP9, PIK3CA, PIK3CB, PIK3R1, RPS6KB1, SRC, VEGFA
hsa05207	Chemical carcinogenesis receptor activation	47.436	1.549×10^{-24}	17	AKT1, AR, BCL2, CYP1A1, CYP1A2, CYP1B1, EGFR, ESR1, ESR2, MTOR, JAK2, PIK3CA, PIK3CB, PIK3R1, RPS6KB1, SRC, VEGFA
hsa04151	PI3K-Akt signaling pathway	30.079	2.264×10^{-22}	18	AKT1, BCL2, BCL2L1, CDK4, EGFR, FGFR1, MTOR, IGF1R, JAK2, KDR, KIT, MET, PIK3CA, PIK3CB, PIK3CG, PIK3R1, RPS6KB1, VEGFA
hsa05224	Breast cancer	56.338	2.498×10^{-21}	14	AKT1, BRAF, CDK4, EGFR, ESR1, ESR2, FGFR1, MTOR, IGF1R, KIT, PIK3CA, PIK3CB, PIK3R1, RPS6KB1
hsa05225	Hepatocellular carcinoma	49.296	1.717×10^{-20}	14	AKT1, BCL2L1, BRAF, CDK4, NQO1, EGFR, MTOR, IGF1R, MET, PIK3CA, PIK3CB, PIK3R1, RPS6KB1, TERT
hsa05215	Prostate cancer	73.181	8.633×10^{-20}	12	AKT1, AR, BCL2, BRAF, EGFR, FGFR1, MTOR, IGF1R, MMP9, PIK3CA, PIK3CB, PIK3R1
hsa05212	Pancreatic cancer	85.619	5.348×10^{-19}	11	AKT1, BCL2L1, BRAF, CDK4, EGFR, MTOR, PIK3CA, PIK3CB, PIK3R1, RPS6KB1, VEGFA

Table 5: Continue

hsa05226	Gastric cancer	47.642	1.805×10^{-17}	12	AKT1, BCL2, BRAF, EGFR, MTOR, MET, ABCB1, PIK3CA, PIK3CB, PIK3R1, RPS6KB1, TERT
hsa04015	Rap1 signaling pathway	36.620	2.336×10^{-17}	13	AKT1, BRAF, EGFR, FGFR1, IGF1R, KDR, KIT, MET, PIK3CA, PIK3CB, PIK3R1, SRC, VEGFA
hsa05218	Melanoma	82.160	3.692×10^{-17}	10	AKT1, BRAF, CDK4, EGFR, FGFR1, IGF1R, MET, PIK3CA, PIK3CB, PIK3R1
hsa05208	Chemical carcinogenesis reactive oxygen species	34.485	5.138×10^{-17}	13	AKT1, BRAF, CYP1A1, CYP1A2, CYP1B1, NQO1, EGFR, MET, PIK3CA, PIK3CB, PIK3R1, SRC, VEGFA
hsa05206	MicroRNAs in cancer	26.715	1.002×10^{-16}	14	BCL2, CYP1B1, DNMT1, EGFR, MTOR, MET, MMP9, ABCC1, ABCB1, PIK3CA, PIK3CB, PIK3R1, PTGS2, VEGFA
hsa04014	Ras signaling pathway	32.724	1.020×10^{-16}	13	AKT1, BCL2L1, EGFR, FGFR1, IGF1R, KDR, KIT, MET, PIK3CA, PIK3CB, PIK3R1, PLA2G2A, VEGFA
hsa05235	PD-L1 expression and PD-1 checkpoint pathway in cancer	66.466	3.428×10^{-16}	10	AKT1, ALK, EGFR, MTOR, JAK2, PIK3CA, PIK3CB, PIK3R1, RPS6KB1, TLR9
hsa04915	Estrogen signaling pathway	47.152	4.981×10^{-16}	11	AKT1, BCL2, EGFR, ESR1, ESR2, MMP2, MMP9, PIK3CA, PIK3CB, PIK3R1, SRC
hsa05418	Fluid shear stress and atherosclerosis	46.813	5.402×10^{-16}	11	AKT1, BCL2, NQO1, KDR, MMP2, MMP9, PIK3CA, PIK3CB, PIK3R1, SRC, VEGFA
hsa04510	Focal adhesion	35.316	6.944×10^{-16}	12	AKT1, BCL2, BRAF, EGFR, IGF1R, KDR, MET, PIK3CA, PIK3CB, PIK3R1, SRC, VEGFA

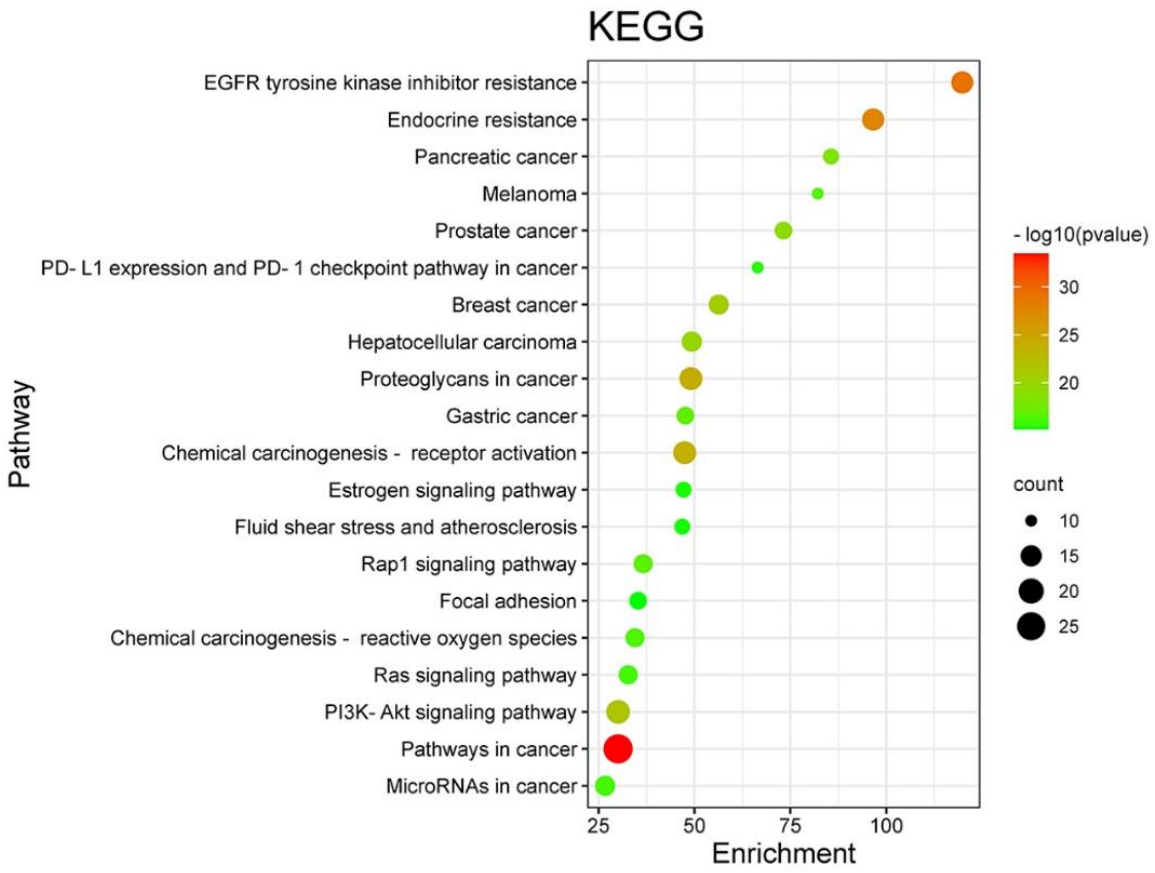

Fig. 5: The result of KEGG pathway enrichment analysis. Horizontal axis: The enrichment; Bubble size: Number of targets enriched in terms; the color represented the p-value

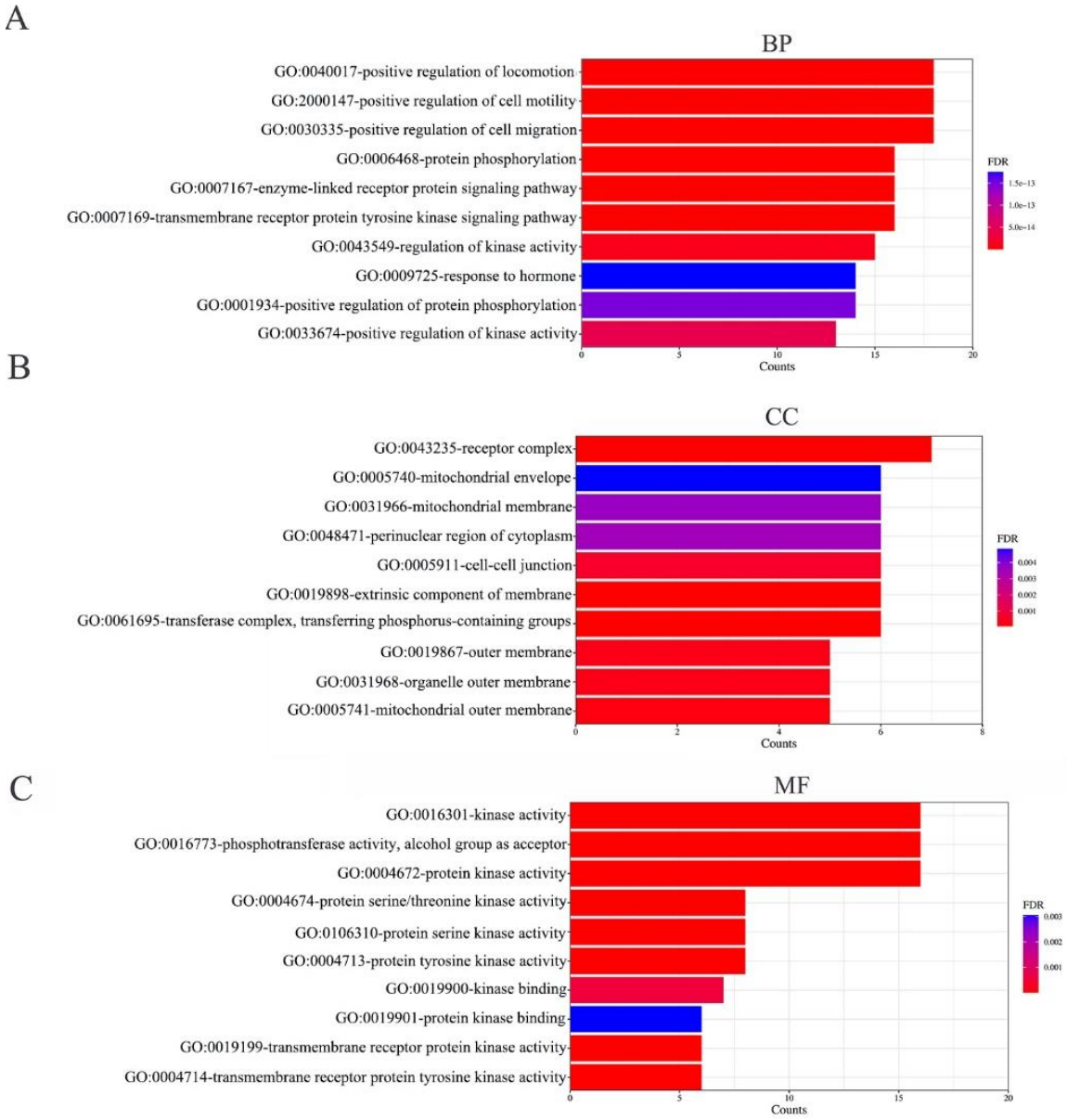

Fig. 6: The results of GO analysis. A: BP analysis, B: CC analysis, and C: MF analysis. Each bar represents a GO entry on the vertical axis, with the number of enriched genes for each term displayed on the horizontal axis. The color of each bar indicated the adjusted p-value (FDR) for the corresponding GO entry

Drug-Targets-Signal Pathways Network

To intuitively reflect the relation between candidate compounds, targets, and signal pathways, the network comprising compounds, targets, and pathways was established (Fig. 8). The 10 candidate compounds connected with 25 targets resulting in 129 component-target associations. Molecule18 and Molecule20 owned the highest number of target associations (degree = 17). Although the number of targets connected to Molecule 19 was the least, it still reached 10. On the other hand, most targets could also connect with more than one compound, such as ESR1, ESR2, KDR, MET, MMP2 and SRC could bind 10 candidate compounds. It indicated that the screened candidate compound had the potential to bind to different targets and the targets would be regulated by different candidate compounds. Moreover, as shown in Fig. 8, all five pathways were connected to different compounds through multiple targets. The results showed that the screened candidate compounds in SB might regulate multi-pathways through multi-targets for CRC treatment which was consistent with the holistic and synergistic characters of TCM.

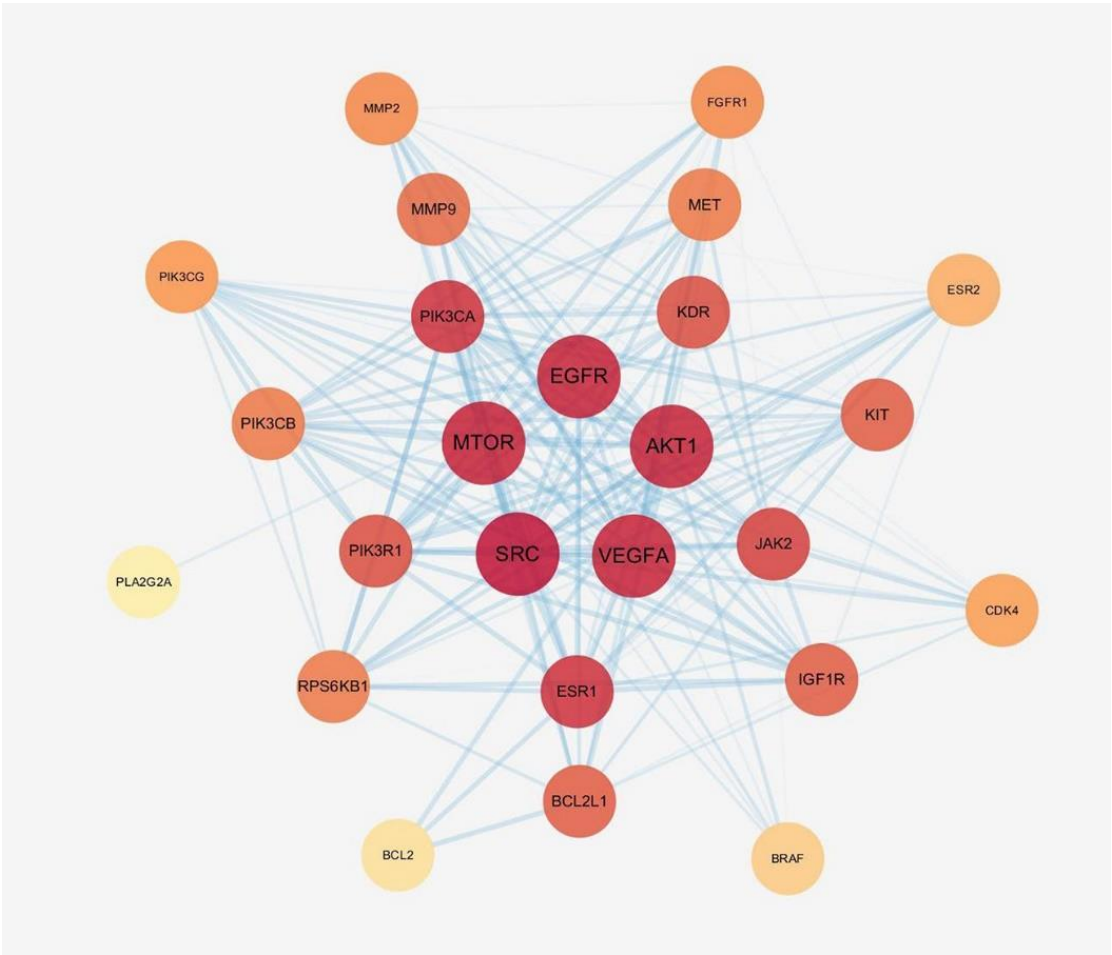

Fig. 7: PPI network of targets associated with selected signaling pathways. The nodes with higher degree owned dark color

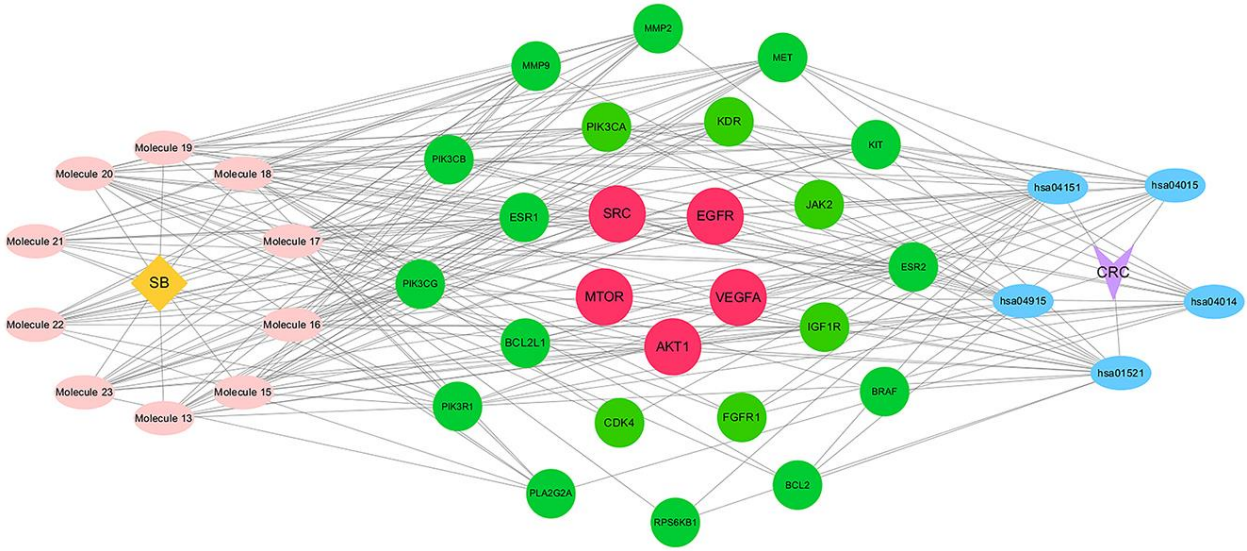

Fig. 8: Relationships between selected signaling pathways, candidate compounds, and targets for the treatment of CRC. Circle nodes represented the targets enriched in selected signaling pathways including five core targets with red color. The pink ovals and blue ovals represented candidate compounds and selected signaling pathways respectively

Expression Changes of Selected Targets in CRC Patients

In total, 8328 DEGs were screened out through PCA analysis and LIMMA analysis and showed in Fig. S2 (Raw data is available upon request from the corresponding author). By overlapping the DEGs and the 25 targets of candidate compounds enriched in selected pathways, a total of 13 targets of candidate compounds expressed differently between the normal group and CRC group which were BCL2, EGFR, FGFR1, KIT, PIK3CG, PLA2G2A, ESR1, ESR2, BCL2L1, MET, VEGFA, CDK4 and MMP9 (Fig. 9). As shown in Fig. 10A, compared with the other four pathways, PI3K-AKT signal pathway mapped most DEGs including BCL2, EGFR, FGFR1, KIT, PIK3CG, BCL2L1, MET, VEGFA and CDK4. Compared with the normal group, the expression of BCL2L1, MET, VEGFA, and CDK4 increased and the BCL2, EGFR, FGFR1, KIT, and PIK3CG were downregulated in CRC groups (Fig. 10B). Based on the results, it could be speculated that modulation of PI3K-AKT signal pathway was the primary mechanism of candidate compounds in SB for the treatment of CRC.

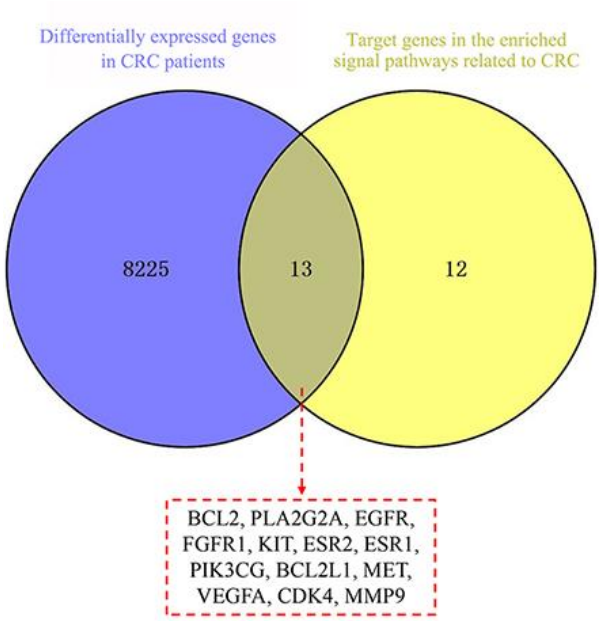

Fig. 9: The screened common DEGs in the selected signaling pathways and the CRC patients

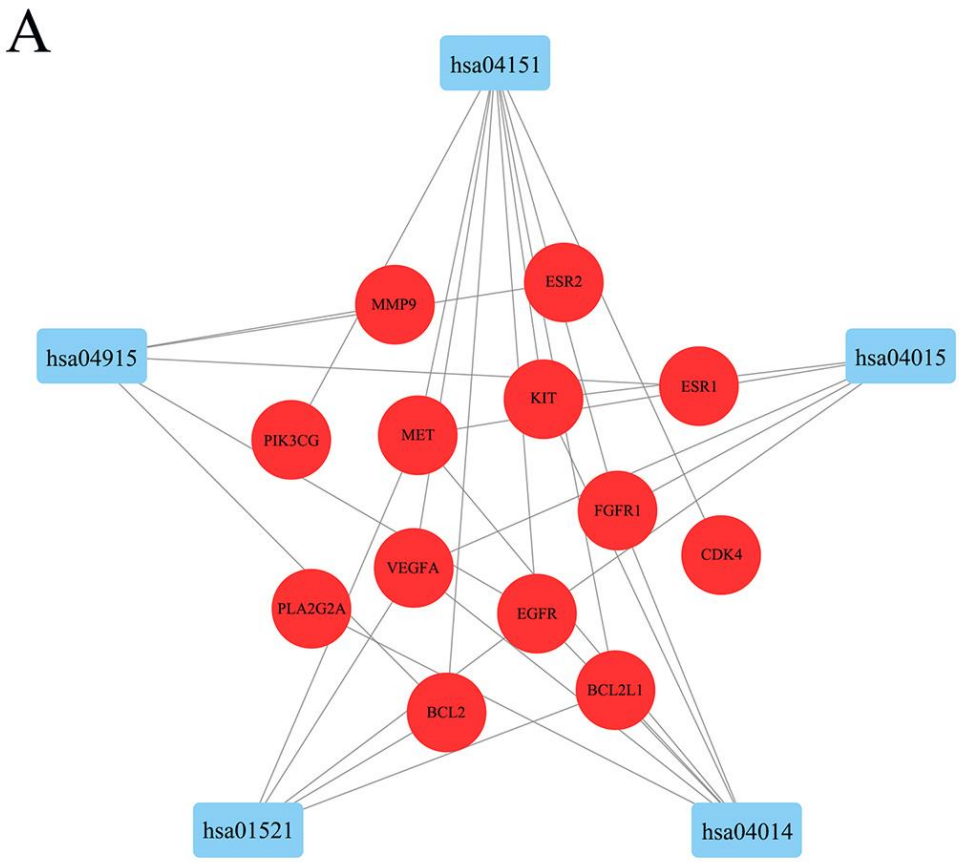

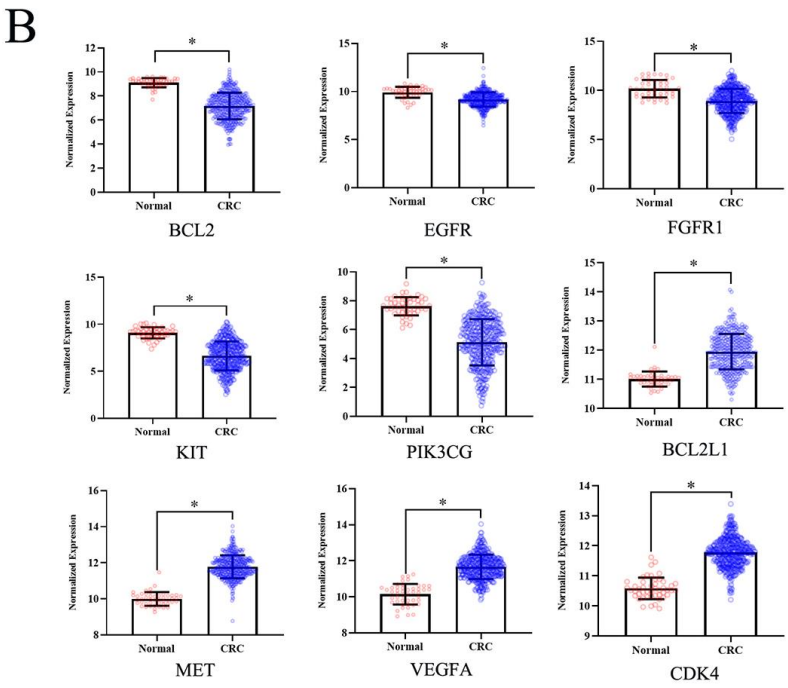

Fig. 10: The expression of screened DEGs and their relationships to selected signaling pathways. (A) Relationships between the screened DEGs and the selected signaling pathways, (B) The screened DEGs of candidate compounds against CRC in the normal and CRC groups. Values were presented as mean ± SD. N = 379 in CRC group and N = 47 in normal group

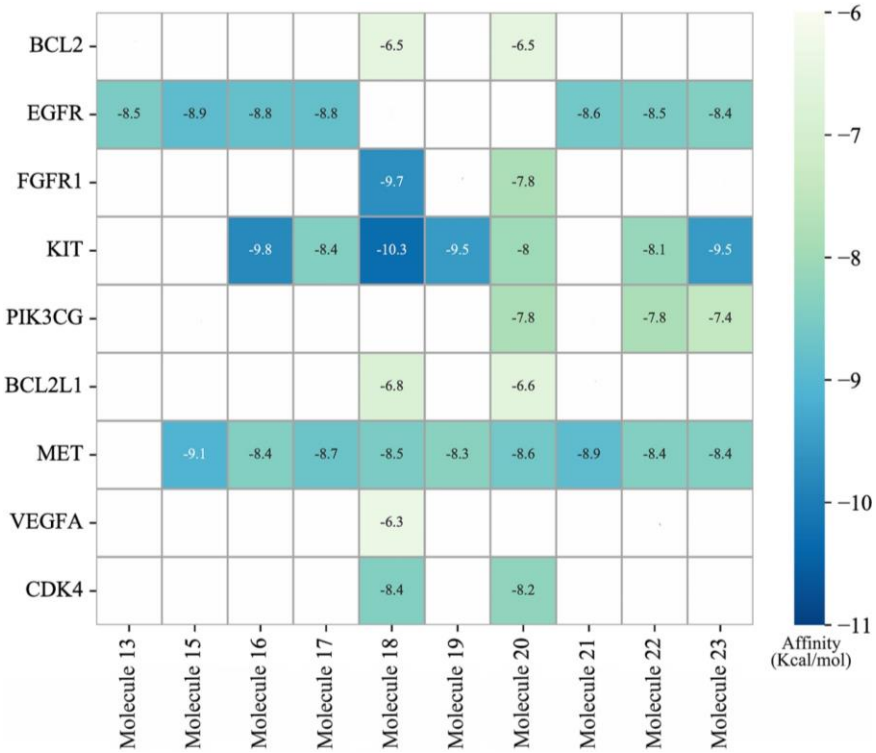

Fig. 11: Molecular docking of screened DEGs and candidate compounds. The colored block charts represented the DEG as the predicted target of the corresponding candidate compounds and the number meant the binding energy. The white block charts meant the DEG was not the predicted target of the corresponding candidate compound

Molecular Docking

In this study, molecular docking analysis was employed to verify the binding ability of candidate compounds with 9 DGEs screened in the PI3K-AKT signaling pathway. Binding free energy (ΔG) can be used to predict the binding capacity between ligands and receptors (Takamatsu *et al*., 2006). Generally, ligands and receptors were considered to bind spontaneously when ΔG was less than 0 Kcal/mol (Leach *et al*., 2006). The lower ΔG value indicated more stable binding between ligand and target. As depicted in Fig. 11, the ΔG values of candidate compounds and their respective targets ranged from -10.3 to -6.3 and the ΔG of most candidate compounds binding to targets were smaller than -7 Kcal/mol indicating the binding configuration with strong activity between candidate compounds and targets (Yang *et al*., 2022). In the group of each target binding to different candidate compounds, interaction owning the smallest ΔG was exhibited in Fig. 12. Molecule18 binding to the amino acid residues in KIT, which showed the minimum ΔG, was through hydrogen bonds, π-bonds, unfavorable Donor-Donor and unfavorable Acceptor-Acceptor. Molecule 15 could dock with EGFR by hydrogen bonds, π-bonds, and unfavorable donor donors. The other targets, such as BCL2, FGFR1, PIK3CG, BCL2L1, MET, VEGFA, and CDK4, interacted with candidate compounds mainly through hydrogen bonds and different π-bonds including Pi-Alkyl bond, Pi-Sigma bond, Pi-Pi bond, Pi-Sulfur bond, and Pi-Anion bond. The results indicated that the candidate compounds could interact with predicted targets by multiple interaction forces that endowed the candidate compounds with a high potential to bond to targets.

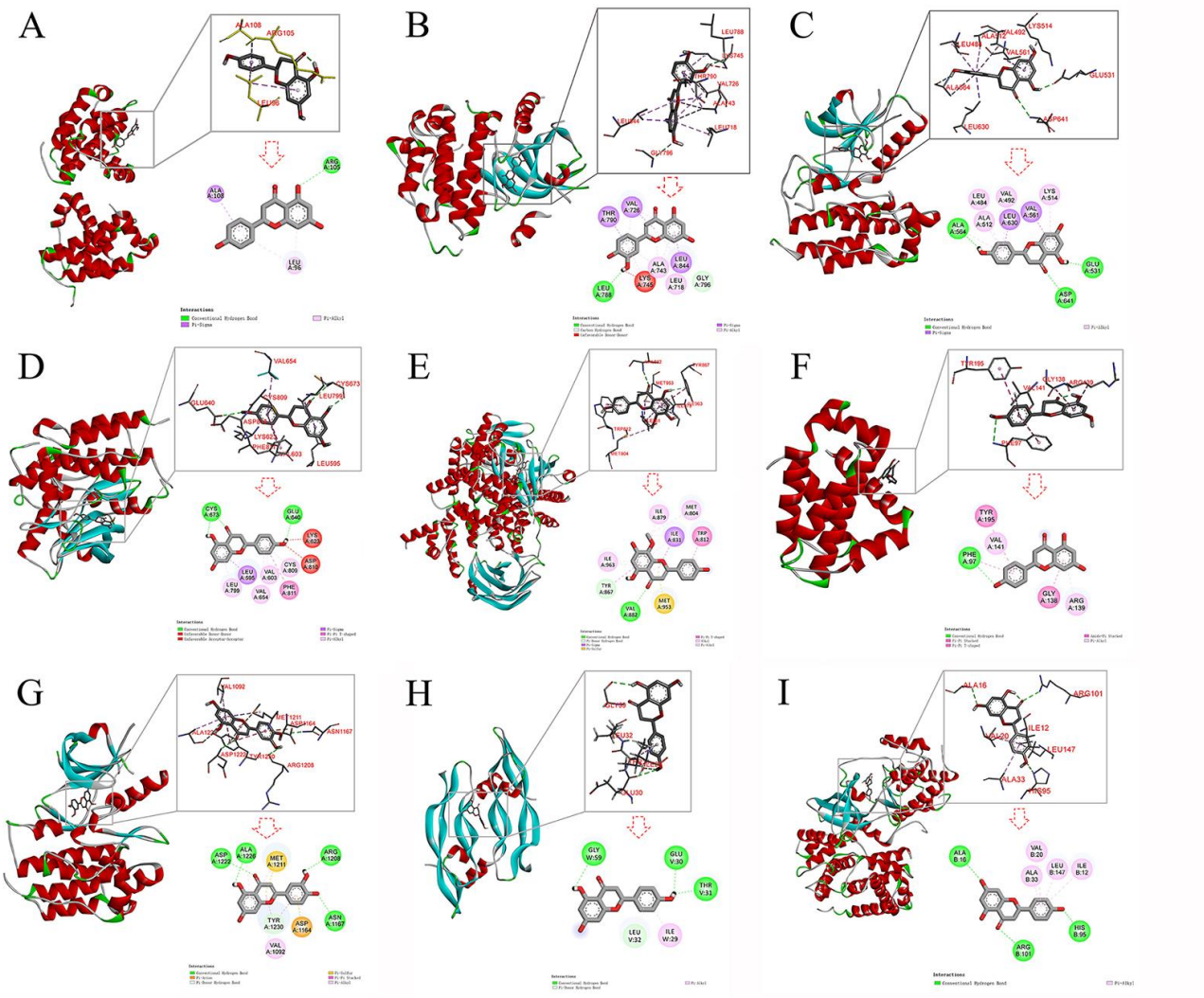

Fig. 12: Molecular docking mode of the screened DEGs and candidate compounds with the lowest binding energy. A: BCL2-Naringenin, B: EGFR-Luteolin, C: FGFR1-Naringenin, D: KIT-Naringenin, E: PIK3CG-4'-hydroxywogonin, F: BCL2L1-Naringenin, G: MET-Luteolin, H: VEGFA-Naringenin, I: CDK4-Naringenin

Discussion

Flavonoids are the major active ingredients in SB, which have a definite therapeutic effect on colorectal cancer (Yang *et al*., 2017). Due to the structural diversity and content difference of flavonoids in SB, the main pharmacodynamic substances for treating CRC and their corresponding pharmacological mechanisms remained unclear. In our study, the chemical profile of SB was initially analyzed by LC-MS. On this basis, candidate flavonoids with therapeutic effects on CRC as well as their targets for CRC treatment were screened out by using network pharmacology and molecular docking techniques.

Oral bioavailability is a crucial factor that influences the further development of active molecules into drugs (Aungst, 2017). The Lipinski rule could accurately predict the absorption or permeability of compounds, which is one of the commonly used empirical rules for drug screening (Van De Waterbeemd *et al*., 2001). In this study, the identified flavonoids in SB were analyzed according to the Lipinski rule. In line with the Lipinski rule is mainly flavonoid aglycones in Table 3. The main reason why flavonoid glycosides do not conform to the Lipinski rule is that there are more hydrogen bond donors and receptors which could induce a large probability of poor absorption or permeability (El-Shafey *et al*., 2020). Traditional Chinese medicine is often taken orally. The structure of flavonoid glycosides has one or more glycosyl groups, with high polarity and low liposolubility. It is difficult to be absorbed in the intestine, resulting in a generally low oral bioavailability. After the flavonoid glycosides are converted into the corresponding aglycones, the polarity becomes smaller, and the liposolubility increases, which can be quickly absorbed into the blood circulation to take effect. For example, baicalin is a 7-O-glucuronide conjugate of baicalein and the reported pharmacokinetic study showed that baicalin exhibited slower and less extensive absorption compared to baicalein (Lai *et al*., 2003). Chen *et al*. (2006) found that, upon oral administration, scutellarin undergoes hydrolysis into scutellarein facilitating enhanced absorption. Based on this, we speculated that the flavonoids in SB were mainly absorbed in the form of aglycones and further exerted the therapeutic effect of CRC.

Based on ADME analysis, ten candidate compounds that comply with Lipinski's five rules were selected from the identified compounds, which proved that these candidate compounds had acceptable pharmacokinetic properties. All the candidate compounds were flavonoid aglycones. Scutellarein is the main flavonoid aglycone in SB, which has a wide range of biological activities against various cancers (Sang Eun *et al*., 2019; Shi *et al*., 2019). It is also the aglycone of scutellarin which was a main flavonoid glycoside in SB. Previous studies have reported that scutellarin can trigger apoptosis in HCT116 cells through a ROS-mediated mitochondrial-dependent pathway (Guo *et al*., 2019). Luteolin is another major flavonoid aglycone in SB which exhibited efficacy against CRC (Imran *et al*., 2019). Previous studies showed that it could block CRC by modulating DNA methyltransferase expression and p53/p21 dependent mechanism (Jang *et al*., 2019; Kang *et al*., 2019). Apigenin, as a natural flavonoid aglycone, possesses numerous biological activities (Singh *et al*., 2022). It has been confirmed that apigenin can significantly promote human colorectal cancer cell apoptosis and anti-proliferation (Yang *et al*., 2021). 4'-Hydroxywogonin, a flavonoid isolated from a variety of plants could inhibit angiogenesis by disrupting the PI3K/AKT pathway for CRC treatment (Sun *et al*., 2018). Hispidulin, a flavonoid owning anti-inflammatory, antifungal, and notably anticancer activities, exerted an anti-CRC effect (Holzner *et al*., 2018; Liu *et al*., 2020). Nargenin was also shown to inhibit human colorectal cell growth by an increase in apoptotic cell death (Abaza *et al*., 2015). That nargenin could be used as an immunomodulator to improve host protection against tumors (Wang *et al*., 2020b). Although direct research about the efficacy of 5, 7, 4'-trihydroxy-8-methoxyflavanone, 8-methoxyluteolin, 6-methoxynaringenin, and 6-methoxyluteolin on CRC has not been reported, it had been verified that these candidate compounds also owned anti-tumor or reversal of chemotherapeutic drug resistance (Li *et al*., 2014; Moharram *et al*., 2021; Tastan *et al*., 2019). Meanwhile, the predicted targets of these four candidate compounds were also enriched in CRC-related pathways (Table 5). It deserves to explore the anti-CRC activity of these four candidate compounds in the future. Furthermore, it was indicated that the candidate compounds had the potential to interact with the active pocket of targets spontaneously with lower binding free energy (Fig. 11). For instance, luteolin could bind to VAL726, LEU788, THR790, and LYS745 in EGFR by various intermolecular interactions shown in Fig. 12B. All the four amino acid residues were key sites in the kinase active pocket of EGFR. VAL726 and LEU788 are located at the bottom of the kinase active pocket, which can control its size and shape thus affecting the binding between targeted therapeutic drugs and EGFR (Lin *et al*., 2017b). THR790 and LYS745 are located at the top of the kinase active pocket. THR790 often participates in inhibitor binding to the active pocket of EGFR (Michalczyk *et al*., 2008). Besides, LYS745 can bind to the inhibitor and stabilize its conformation, thus effectively blocking the activity of EGFR (Klatt *et al*., 2013). These amino acid sites are of great significance for the design and development of EGFR-targeted drugs. Consequently, it was speculated that these 10 candidate compounds may be the pharmacodynamic ingredients in SB for CRC treatment.

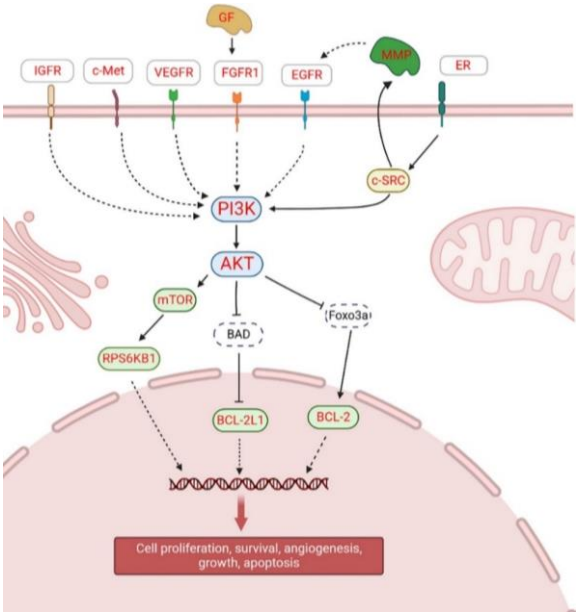

Fig. 13: The predicted pathway depicting the restraint of CRC by candidate compounds in SB. Red font indicates the predicted targets of candidate compounds

To clarify the potential pharmacological mechanisms of candidate compounds in CRC treatment, a KEGG pathway enrichment analysis was conducted. It revealed that, besides CRC, the targets of candidate compounds had a relationship with various cancer (Tables S1-S5) (appendix will be available on request to author), which was consistent with the broad anti-cancer activities of SB previously reported (Sheng *et al*., 2022; Wang *et al*., 2019; Zheng *et al*., 2018). Through systematically analyzing the targets of candidate compounds in these five pathways, it was found that these targets were mainly the upstream receptors, downstream effectors, and core targets of the PI3K-AKT pathway (Fig. 13). In addition, among the top 10 core targets identified in the PPI network, eight were found to be associated with the PI3K-AKT signaling pathway. Previous studies have demonstrated the crucial involvement of the PI3K-AKT signaling pathway in promoting the proliferation and metastasis of CRC (Jiang *et al*., 2021). Lin *et al*., revealed that the extracts of SB could inhibit proliferation and enhance apoptosis in HCT-8/5-FU cells which was due to the suppression of the PI3K/AKT pathway activation (Lin *et al*., 2017c). Thus, it suggested that the candidate compounds may function for the treatment of CRC mainly by regulating the PI3K-AKT signaling pathway. In cancer, the activation of upstream receptors is crucial for the proper functioning of the PI3K-AKT signaling pathway. In this research, it was found that some targets of candidate compounds were the upstream receptors of the PI3K-AKT signaling pathway which mainly belonged to the RTK family, including EGFR, VEGFA, and FGFR1 (He *et al*., 2021). These receptors are transmembrane proteins with intrinsic phosphotyrosine kinase activity and they can activate the PI3K-AKT signaling pathway by binding to ligands to regulate cell survival, angiogenesis, and metabolism in cancer progression (Sangwan and Park, 2006). It was in accordance with the results of GO enrichment analysis. As shown in Figure 6, BP analysis enriched transmembrane receptor protein tyrosine kinase signaling pathway (GO:0007169) and MF analysis enriched transmembrane receptor protein tyrosine kinase activity (GO:0004714). EGFR is a receptor tyrosine kinase that phosphorylates tyrosine residues and activates the PI3K-Akt signaling pathway by binding to ligands. When the anti-EGFR monoclonal antibody competitively binds to EGFRs, it suppresses cancer occurrence and development by inhibiting the PI3K-Akt signaling pathway (Liu *et al*., 2001). According to previous reports, naringenin, a flavonoid aglycone present in SB, has been shown to inhibit the activation of EGFR, subsequently leading to the depression of the PI3K-Akt signaling pathway (Yang *et al*., 2011). Scutellarein, the main flavonoid aglycone in SB, could also depress the expression levels of phosphorylated EGFR to inhibit cancer cell proliferation (Cheng *et al*., 2014). VEGFA is a growth factor owning an intracellular tyrosine kinase domain and activating in angiogenesis. It has been shown that VEGFA can influence vasculogenic mimicry to promote CRC metastasis and progression via activating the PI3K/AKT signaling pathway and it was found that apigenin could decrease VEGF expression to suppress tumor angiogenesis (Fang *et al*., 2007; Liu *et al*., 2022b). FGFR1 is a tyrosine-protein kinase that plays a very important role in cancer metastasis and angiogenesis. Tang *et al*. (2018) found that silencing the expression of FGFR1 at the protein level could inhibit PI3K/AKT signaling and subsequently suppress bone metastasis of prostate cancer. Luteolin could also induce dramatic down-regulation of FGFR1 (Chen *et al*., 2018b). In the research, some downstream effectors of the PI3K/AKT signaling pathway, such as mTOR, RPS6KB1, BCL2, and BCL2L, were also screened out as the potential targets of candidate compounds. mTOR is known to act as serine/threonine protein kinase and tyrosine kinase, respectively. The activation of the mTOR signaling pathway has been shown to enhance growth factor receptor signaling, promote angiogenesis, facilitate cancer cell migration, and inhibit autophagy (Hua *et al*., 2019). These effects could collectively promote tumor growth and progression. It is implicated in human colorectal cancer (Silva *et al*., 2021). Yang *et al*. (2010) showed that hispidulin treatment resulted in mTOR inhibition in ovarian cancer cells. RPS6KB1 acts as a

downstream effector of mTOR signaling to facilitate cell proliferation and cycle progression. In CRC, phosphorylated RPS6KB1 can regulate protein synthesis and promote cell survival by inhibiting pro-apoptotic pathways (An *et al*., 2019). The anti-apoptotic proteins BCL-2 and BCL-2 L1 can promote malignant cell survival by attenuating apoptosis (Ashkenazi *et al*., 2017). Previously, Liu *et al*. (2022a) found that the flavonoids extracted from SB could inhibit cell proliferation and promote apoptosis in HCT116 cells by down-regulating BCL-2. In addition, we found that half of the candidate compound targets enriched in the PI3K-AKT pathway are differently expressed in CRC patients by analyzing the RNA sequencing data in the TCGA database. Therefore, it could be presumed that, by interacting with upstream receptors, downstream effectors, and targets in the PI3K-AKT pathway, the candidate compounds exerted anti-proliferative and anti-angiogenic effects, as well as the facilitation of cancer cell apoptosis, for treating CRC.

Conclusion

In this study, a comprehensive analysis revealed 25 distinct major flavonoids in SB by HPLC-QTOF-MS/MS, and 10 flavonoid aglycones with good ADME characters were screened out as candidate compounds. Through bioinformatics analysis, it indicated that the candidate compounds had the potential to inhibit cell proliferation and angiogenesis while promoting cancer cell apoptosis. These effects were primarily mediated through the regulation of PI3K-AKT pathway, as well as the modulation of upstream receptors and downstream effectors. These therapeutic implications of candidate compounds were significant for suppressing the occurrence and progression of CRC. In summary, our current findings clearly demonstrate that the screened flavonoid aglycones may be the main pharmacodynamic ingredients in SB for the treatment of CRC, mainly by regulating the PI3K-AKT pathway, and have great potential in application for developing drugs against CRC.

Acknowledgment

Thank you to the publisher for their support in the publication of this research article. We are grateful for the resources and platform provided by the publisher, which have enabled us to share our findings with a wider audience. We appreciate the effort of the editorial team in reviewing and editing our work, and we are thankful for the opportunity to contribute to the field of research through this publication.

Funding Information

This research was funded by the national natural science foundation of China (82003885), the Suzhou science and technology development project (SKJYD2021149), the foreign academician workstation of Suzhou City (SWY2020001), and the Suzhou science and technology plan project (SNG2021005).

Author's Contributions

Yi-Jie Cheng: Conceptualization, methodology, written, original drifted preparation, funded acquisition.

Xin-Yun Du and Rui-Huan Chen: Investigation.

Jing-Yuan Xu: Conceptualization, written, reviewed and edited, funded acquisition.

Ai-Guo Zhu: Software.

Bo Jiang: Visualization and funded acquisition.

Xia Tian: Software, supervision, and funded acquisition.

Ethics

This article is original and contains unpublished material. The corresponding author confirms that all of the other authors have read and approved the manuscript and that no ethical issues are involved.

References

Abaza, M. S. I., K. Y. Orabi, E. Al-Quattan & R. J. Al-Attiyah. (2015). Growth inhibitory and chemo-sensitization effects of naringenin, a natural flavanone purified from Thymus vulgaris, on human breast and colorectal cancer. *Cancer Cell International*, *15*, 46. https://doi.org/10.1186/s12935-015-0194-0

An, H. J., Park, M. Kim, J., & Han. Y. H. (2019). miR-5191 functions as a tumor suppressor by targeting RPS6KB1 in colorectal cancer. *International Journal of Oncology*, *55*(4): 960-972. https://doi.org/10.3892/ijo.2019.4865

Ashkenazi, A., Fairbrother, W. J. Leverson, J. D., & A. J. Souers. (2017). From basic apoptosis discoveries to advanced selective BCL-2 family inhibitors. Nature Reviews. *Drug Discovery*, *16*(4): 273-284. https://doi.org/10.1038/nrd.2016.253

Aungst, B. J. (2017). Optimizing Oral Bioavailability in Drug Discovery: An Overview of Design and Testing Strategies and Formulation Options. *Journal of Pharmaceutical Sciences*, *106*(4): 921-929. https://doi.org/10.1016/j.xphs.2016.12.002

Bi, Y., Han, X. Lai, Y. Fu, Y. Li, K. Zhang, W. Wang, Q. Jiang, X. Zhou, Y. Liang, H., & Fan, H. (2021). Systems pharmacological study based on UHPLC-Q-Orbitrap-HRMS, network pharmacology and experimental validation to explore the potential mechanisms of Danggui-Shaoyao-San against atherosclerosis. *Journal of Ethnopharmacology*, *278*: 114278. https://doi.org/10.1016/j.jep.2021.114278

Biller, L. H., & Schrag, D. (2021). Diagnosis and Treatment of Metastatic Colorectal Cancer: A Review. *JAMA*, *325*(7): 669-685. https://doi.org/10.1001/jama.2021.0106

Cartwright, T. H. (2012). Treatment Decisions After Diagnosis of Metastatic Colorectal Cancer. *Clinical Colorectal Cancer*, *11*(3): 155-166. https://doi.org/10.1016/j.clcc.2011.11.001

Chen, D., Zhao, J., & Cong, W. (2018a). Chinese Herbal Medicines Facilitate the Control of Chemotherapy-Induced Side Effects in Colorectal Cancer: Progress and Perspective. *Frontiers in Pharmacology*, *9*: 1442. https://doi.org/10.3389/fphar.2018.01442

Chen, P. Y., Tien, H. J., Chen, S. F., Horng, C. T., Tang, H. L., Jung, H. L., Wu, M. J., & Yen. J. H. (2018b). Response of Myeloid Leukemia Cells to Luteolin is Modulated by Differentially Expressed Pituitary Tumor-Transforming Gene 1 (PTTG1) Oncoprotein. *International Journal of Molecular Sciences*, *19*(4): 1173. https://doi.org/10.3390/ijms19041173

Chen, X., Cui, L. Duan, X. Ma B., & Zhong, D. (2006). Pharmacokinetics and metabolism of the flavonoid scutellarin in humans after a single oral administration. Drug Metabolism and *Disposition: The Biological Fate of Chemicals*, *34*(8): 1345-1352. https://doi.org/10.1124/dmd.106.009779

Cheng, C. Y., Hu, C. C., Yang, H. J., Lee, M. C., & Kao, E. S. (2014). Inhibitory effects of scutellarein on proliferation of human lung cancer A549 cells through ERK and NFκB mediated by the EGFR pathway. *The Chinese Journal of Physiology*, *57*(4): 182-187. https://doi.org/10.4077/CJP.2014.BAC200

Cheng, Y., Zhang, Y. Sun, H. Huang, D. Jiang, B., & Xu, J. (2022). Optimization of Ultrasonic-Assisted Total Flavonoids Extraction from Flower of Albizia Julibrissin Durazz. by Response Surface Methodology for Characterization of Chemical Profile and Evaluation of Antioxidant and Tyrosinase Inhibitory Activities. *American Journal of Biochemistry and Biotechnology*, *18*(1): 100-117. https://doi.org/10.3844/ajbbsp.2022.100.117

Daina, A., Michielin, O., & Zoete, V. (2019). SwissTargetPrediction: Updated data and new features for efficient prediction of protein targets of small molecules. *Nucleic Acids Research*, *47*(W1): W357-W364. https://doi.org/10.1093/nar/gkz382

Daina, A., Michielin, O., & Zoete, V. (2017). SwissADME: A free web tool to evaluate pharmacokinetics, drug-likeness and medicinal chemistry friendliness of small molecules. *Scientific Reports*, *7*: 42717. https://doi.org/10.1038/srep42717

Dekker, E., Tanis, P. J. Vleugels, J. L. A. Kasi, P. M., & Wallace, M. B. (2019). Colorectal cancer. *Lancet*, *394*(10207): 1467-1480. https://doi.org/10.1016/S0140-6736(19)32319-0

El-Shafey, H. W., Gomaa, R.M. El-Messery, S. M., & Goda, F. E. (2020). Quinazoline Based HSP90 Inhibitors: Synthesis, Modeling Study and ADME Calculations Towards Breast Cancer Targeting. *Bioorganic and Medicinal Chemistry Letters*, *30*(15): 127281. https://doi.org/10.1016/j.bmcl.2020.127281

Fan, H., Liu, S. Shen, W. Kang, A. Tan, J. Li, L. Liu, X. Xu, C. Xu, X. Lai, Y. Cheng, H., & Sun, D. (2020). Identification of the absorbed components and metabolites of Xiao-Ai-Jie-Du decoction and their distribution in rats using ultra high-performance liquid chromatography/quadrupole time-of-flight mass spectrometry. *Journal of Pharmaceutical and Biomedical Analysis*, *179*: 112984. https://doi.org/10.1016/j.jpba.2019.112984

Fang, J., Zhou, Q. Liu, L.Z. Xia, C. Hu, X. Shi X., & Jiang, B., H. (2007). Apigenin inhibits tumor angiogenesis through decreasing HIF-1alpha and VEGF expression. *Carcinogenesis 28*(4): 858-864. https://doi.org/10.1093/carcin/bgl205

Guo, F., Yang F., & Zhu, Y. H. (2019). Scutellarein from *Scutellaria barbata* induces apoptosis of human colon cancer HCT116 cells through the ROS-mediated mitochondria-dependent pathway. *Natural Product Research*, *33*(16): 2372-2375. https://doi.org/10.1080/14786419.2018.1440230

Hay, M. Thomas, D. W. Craighead, J. L. Economides, C., & Rosenthal, J. (2014). Clinical development success rates for investigational drugs. *Nature Biotechnology*, *32*(1): 40-51. https://doi.org/10.1038/nbt.2786

He, Y., Sun, M. M. Zhang, G. G. Yang, J. Chen, K. S. Xu, W. W., & Li, B. (2021). Targeting PI3K/Akt signal transduction for cancer therapy. *Signal Transduction and Targeted Therapy*, *6*(1): 425. https://doi.org/10.1038/s41392-021-00828-5

Holzner, S., Brenner, S. Atanasov, A. G. Senfter, D. Stadler, S. Nguyen, C. H. Fristiohady, A. Milovanovic, D. Huttary, N. Krieger, S. Bago-Horvath, Z. de Wever, O. Tentes, I. Özmen, A. Jäger, W. Dolznig, H. Dirsch, V. M. Mader, R. M. Krenn, L., & Krupitza, G. (2018). Intravasation of SW620 colon cancer cell spheroids through the blood endothelial barrier is inhibited by clinical drugs and flavonoids *in vitro*. *Food and Chemical Toxicology*, *111*: 114-124. https://doi.org/10.1016/j.fct.2017.11.015

Hua, H., Kong, Zhang, Q. Wang, H. Luo, J., & Jiang, T. Y. (2019). Targeting mTOR for cancer therapy. *Journal of Hematology and Oncology*, *12*(1): 71. https://doi.org/10.1186/s13045-019-0754-1

Imran, M., Rauf, A. Abu-Izneid, T. Nadeem, M. Shariati, M. A. Khan, I. A. Imran, A. Orhan, I. E. Rizwan, M. Atif, M. Gondal, T. A., & Mubarak, M. S. (2019). Luteolin, a flavonoid, as an anticancer agent: A review. *Biomedicine & Pharmacotherapy*, *112*: 108612. https://doi.org/10.1016/j.biopha.2019.108612

Jang, C.H., Moon, N. Oh, J., & Kim, J. S. (2019). Luteolin Shifts Oxaliplatin-Induced Cell Cycle Arrest at G_0/G_1 to Apoptosis in HCT116 Human Colorectal Carcinoma Cells. *Nutrients*, *11*(4): 770. https://doi.org/10.3390/nu11040770

Jiang, T., Wang, H. Liu, L. Y. Song, H. Zhang, Y. Wang, J. Liu, L. Xu, T. Fan, R. Xu, Y. Wang, S. Shi, L. Zheng, L. Wang, R., & Song, J. (2021). CircIL4R activates the PI3K/AKT signaling pathway via the miR-761/TRIM29/PHLPP1 axis and promotes proliferation and metastasis in colorectal cancer. *Molecular Cancer*, *20*(1): 167. https://doi.org/10.1186/s12943-021-01474-9

Kang, A., Jiang, J. Li, Q. Sheng, X. Chen, Y. Tan, J. Li, L. Shen, W. Tang, D. Cheng, H., & Sun, D. (2022). Characterization of the chemical constituents and *in vivo* metabolic profile of *Scutellaria barbata* D. Don by ultra high performance liquid chromatography with high-resolution mass spectrometry. *Journal of Separation Science*, *45*(9): 1600-1609. https://doi.org/10.1002/jssc.202100852

Kang, K. Piao, A., Hyun, M. Zhen, J. Cho, Y. J. Ahn, A. X. S. J. M. J. Yi, J. M., & Hyun, J. W. (2019). Luteolin promotes apoptotic cell death via upregulation of Nrf2 expression by DNA demethylase and the interaction of Nrf2 with p53 in human colon cancer cells. *Experimental & Molecular Medicine*, *51*(4): 1-14. https://doi.org/10.1038/s12276-019-0238-y

Klatt, N. R., Canary, L. A. Sun, X. Vinton, C. L. Funderburg, N. T. Morcock, D. R. Quiñones, M. Deming, C. B. Perkins, M. Hazuda, D. J. Miller, M. D. Lederman, M. M. Segre, J. A. Lifson, J. D. Haddad, E. K. Estes, J. D., & Brenchley, J. M. (2013). Probiotic/prebiotic supplementation of antiretrovirals improves gastrointestinal immunity in SIV-infected macaques. *The Journal of Clinical Investigation*, *123*(2): 903-907. https://doi.org/10.1172/JCI66227

Lai, M. Y., Hsiu, S. L. Tsai, S. Y. Hou, Y.C., & P. D. Chao, L. (2003). Comparison of metabolic pharmacokinetics of baicalin and baicalein in rats. *The Journal of Pharmacy and Pharmacology*, *55*(2): 205-209. https://doi.org/10.1211/002235702522

Leach, A. R., Shoichet, B. K., & Peishoff, C. E. (2006). Prediction of protein-ligand interactions. Docking and scoring: successes and gaps. *Journal of Medicinal Chemistry*, *49*(20): 5851-5855. https://doi.org/10.1021/jm060999m

Li, J., Wang, Y. Lei, J. C. Hao, Y. Yang, Y. Yang, C. X., & Yu, J. Q. (2014). Sensitisation of ovarian cancer cells to cisplatin by flavonoids from *Scutellaria barbata*. *Natural Product Research*, *28*(10): 683-689. https://doi.org/10.1080/14786419.2013.871547

Li, R., Song, W. Qiao, X. Liu, J. Liang, H., & Ye, M. (2015). Chemical profiling of *Scutellaria barbata* by ultra-high performance liquid chromatography coupled with hybrid quadrupole-orbitrap mass spectrometry. *Journal of Chinese Pharmaceutical Sciences*, *24*(10) 635-646. https://doi.org/10.5246/jcps.2015.10.081

Li, S., Lin, Z. Jiang, H. Tong, L. Wang, H., & Chen, S. (2016). Rapid Identification and Assignation of the Active Ingredients in Fufang Banbianlian Injection Using HPLC-DAD-ESI-IT-TOF-MS. *Journal of Chromatographic Science*, *54*(7): 1225-1237. https://doi.org/10.1093/chromsci/bmw055

Li, X., Wei, S. Niu, S. Ma, X. Li, H. Jing, M., & Zhao, Y. (2022). Network pharmacology prediction and molecular docking-based strategy to explore the potential mechanism of Huanglian Jiedu Decoction against sepsis. *Computers in Biology and Medicine*, *144*: 105389. https://doi.org/10.1016/j.compbiomed.2022.105389

Li, Y., Wang, J. Zhong, S. Li, J., & Du, W. (2020). Scutellarein inhibits the development of colon cancer via CDC4-mediated RAGE ubiquitination. *International Journal of Molecular Medicine*, *45*(4): 1059-1072. https://doi.org/10.3892/ijmm.2020.4496

Lin, F., Li, F. Wang, C. Wang, J. Yang, Y. Yang, L., & Li. Y. (2017a). Mechanism Exploration of Arylpiperazine Derivatives Targeting the 5-HT2A Receptor by In Silico Methods. *Molecules*, *22*(7): 1064. https://doi.org/10.3390/molecules22071064

Lin, J., Feng, J. Yang, H. Yan, Z. Li, Q. Wei, L. L. Lai, Z. Jin, Y., & Peng, J. (2017b). *Scutellaria barbata* D. Don inhibits 5-fluorouracil resistance in colorectal cancer by regulating PI3K/AKT pathway. *Oncology Reports*, *38*(4): 2293-2300. https://doi.org/10.3892/or.2017.5892

Lin, T. H., Yen, H. R. Chiang, J. H. Sun, M. F. Chang, H. H., & Huang, S. T. (2017c). The use of Chinese herbal medicine as an adjuvant therapy to reduce incidence of chronic hepatitis in colon cancer patients: A Taiwanese population-based cohort study. *Journal of Ethnopharmacology*. *202*: 225-233. https://doi.org/10.1016/j.jep.2017.03.027

Liu, B., Fang, M. Lu, Y. Mendelsohn, J., & Fan, Z. (2001). Fibroblast growth factor and insulin-like growth factor differentially modulate the apoptosis and G1 arrest induced by anti-epidermal growth factor receptor monoclonal antibody. *Oncogene 20*(15): 1913-1922. https://doi.org/10.1038/sj.onc.1204277

Liu, K., Zhao, F. Yan, J. Xia, Z. Jiang, D., & Ma, P. (2020). Hispidulin: A promising flavonoid with diverse anti-cancer properties. *Life Sciences*, *259*: 118395. https://doi.org/10.1016/j.lfs.2020.118395

Liu, L., Liu, T. Tao, W. Liao, N. Yan, Q. L. Li, J. Tan, W. Shen, Cheng, H., & Sun, D. (2022a). Flavonoids from *Scutellaria barbata* D. Don exert antitumor activity in colorectal cancer through inhibited autophagy and promoted apoptosis via ATF4/sestrin2 pathway. *Phytomedicine*, *99*: 154007. https://doi.org/10.1016/j.phymed.2022.154007

Liu, X., He, H. Zhang, F. Hu, X. Bi, F. Li, K. Yu, H. Zhao, Y. Teng, X. Li, J. Wang, L. Zhang, Y., & Wu, Q. (2022b). m6A methylated EphA2 and VEGFA through IGF2BP2/3 regulation promotes vasculogenic mimicry in colorectal cancer via PI3K/AKT and ERK1/2 signaling. *Cell Death & Disease*, *13*(5): 483. https://doi.org/10.1038/s41419-022-04950-2

Michalczyk, A., Klüter, S. Rode, H. B. Simard, J. R. Grütter, C. Rabiller, M., & Rauh, D. (2008). Structural insights into how irreversible inhibitors can overcome drug resistance in EGFR. *Bioorganic & Medicinal Chemistry*, *16*(7): 3482-3488. https://doi.org/10.1016/j.bmc.2008.02.053

Moharram, F. A., Nagy, M. M. El Dib, R. A. El-Tantawy, M. M. El Hossary, G. G., & El-Hosari, D. G. (2021). Pharmacological activity and flavonoids constituents of Artemisia judaica L aerial parts. *Journal of Ethnopharmacology*, *270*: 113777. https://doi.org/10.1016/j.jep.2021.113777

Sang Eun, H., Seong, K. Min, L. Ho Jeong, P. Vetrivel, V. Venkatarame Gowda Saralamma, H. Jeong Doo, K. Eun Hee, L. Sang Joon & Gon Sup, K. (2019). Scutellarein Induces Fas-Mediated Extrinsic Apoptosis and G2/M Cell Cycle Arrest in Hep3B Hepatocellular Carcinoma Cells. *Nutrients*, *11*(2): 263. https://doi.org/10.3390/nu11020263

Sangwan, V. & Park. M. (2006). Receptor tyrosine kinases: Role in cancer progression. *Current Oncology*, *13*(5): 191-193. https://doi.org/10.3390/curroncol13050019

Sawicki, T., Ruszkowska, M. Danielewicz, A. Niedźwiedzka, E. Arłukowicz, T., & Przybyłowicz, K. E. (2021). A Review of Colorectal Cancer in Terms of Epidemiology, Risk Factors, Development, Symptoms and Diagnosis. *Cancers (Basel)*. *13*(9): 2025. https://doi.org/10.3390/cancers13092025

Shang, L., Wang, Y. Li, J. Zhou, F. Xiao, K. Liu, Y. Zhang, M. Wang, S., & Yang, S. (2023). Mechanism of Sijunzi Decoction in the treatment of colorectal cancer based on network pharmacology and experimental validation. *Journal of Ethnopharmacology*, *302*(PartA): 115876. https://doi.org/10.1016/j.jep.2022.115876

Sheng, D., Zhao, B. Zhu, W. Wang, T., & Peng, Y. (2022). *Scutellaria barbata* D. Don (SBD) extracts suppressed tumor growth, metastasis and angiogenesis in Prostate cancer via PI3K/Akt pathway. *BMC Complementary Medicine and Therapies*, *22*(1): 120. https://doi.org/10.1186/s12906-022-03587-0

Shi, L., Wu, Y. Lv, D. L., & Feng, L. (2019). Scutellarein selectively targets multiple myeloma cells by increasing mitochondrial superoxide production and activating intrinsic apoptosis pathway. *Biomedicine & Pharmacotherapy*, *109*: 2109-2118. https://doi.org/10.1016/j.biopha.2018.09.024

Silva, V. R., Santos, L. de, S. Dias, R. B. Quadros, C.A., & Bezerra, D. P. (2021). Emerging agents that target signaling pathways to eradicate colorectal cancer stem cells. *Cancer Communications*, *41*(12): 1275-1313. https://doi.org/10.1002/cac2.12235

Singh, D., Gupta, M. Sarwat, M., & Siddique, H. R. (2022). Apigenin in cancer prevention and therapy: A systematic review and meta-analysis of animal models. *Critical Reviews in Oncology/Hematology*, *176*: 103751. https://doi.org/10.1016/j.critrevonc.2022.103751

Sun, D., Zhang, F. Qian, J. Shen, W. Fan, H. Tan, J. Li, L. Xu, C. Yang, Y., & Cheng, H. (2018). 4'-hydroxywogonin inhibits colorectal cancer angiogenesis by disrupting PI3K/AKT signaling. *Chemico-Biological Interactions*, *296*: 26-33. https://doi.org/10.1016/j.cbi.2018.09.003

Szklarczyk, D., Gable, A. L. Lyon, D. Junge, A. Wyder, S. Huerta-Cepas, J. Simonovic, M. Doncheva, N. T. Morris, J. H. Bork, P. Jensen, L. J., & Von Mering, C. (2019). STRING v11: protein-protein association networks with increased coverage, supporting functional discovery in genome-wide experimental datasets. *Nucleic Acids Research*, *47*(D1): D607-D613. https://doi.org/10.1093/nar/gky1131

Takamatsu, Y., Sugiyama, A. Purqon, A. Nagao, H., & Nishikawa. K. (2006). Binding Free Energy Calculation and Structural Analysis for Antigen-Antibody Complex. *AIP Conference Proceedings*, *832*(1): 566-569. https://doi.org/10.1063/1.2204566

Tang, Y., Pan, J. Huang, S. Peng, X. Zou, X. Luo, Y. Ren, D. Zhang, X. Li, R. He, P., & Wa, Q. (2018). Downregulation of miR-133a-3p promotes prostate cancer bone metastasis via activating PI3K/AKT signaling. *Journal of Experimental and Clinical Cancer Research*: CR, *37*(1), 160. https://doi.org/10.1186/s13046-018-0813-4

Tastan, P., Hajdú, Z. Kúsz, N. Zupkó, I. Sinka, I. Kivcak, B., & Hohmann, J. (2019). Sesquiterpene Lactones and Flavonoids from Psephellus pyrrhoblepharus with Antiproliferative Activity on Human Gynecological Cancer Cell Lines. *Molecules 24*(17): 3165. https://doi.org/10.3390/molecules24173165

Van De Waterbeemd, H., Smith, K. Beaumont & Walker, D. K. (2001). Property-based design: Optimization of drug absorption and Pharmacokinetics. *Journal of Medicinal Chemistry*, *44*(9): 1313-1333. https://doi.org/10.1021/jm000407e

Wang, L., Xu, J. Yan, Y. Liu, H. Karunakaran, T., & Li, F. (2019). Green synthesis of gold nanoparticles from *Scutellaria barbata* and its anticancer activity in pancreatic cancer cell (PANC-1). *Artificial Cells, Nanomedicine and Biotechnology*, *47*(1): 1617-1627. https://doi.org/10.1080/21691401.2019.1594862

Wang, L., Chen, W. Li, M. Zhang, F. Chen, K., & Chen, W. S. (2020a). A review of the ethnopharmacology, phytochemistry, pharmacology and quality control of *Scutellaria barbata* D. Don. *Journal of Ethnopharmacology*, *254*: 112260. https://doi.org/10.1016/j.jep.2019.112260

Wang, L. Y., Zeng, W. Wang, L. Y. Wang, Z. Yin, X. Qin, Y. Zhang, F. Zhang, C., & Liang, W. (2020b). Naringenin Enhances the Antitumor Effect of Therapeutic Vaccines by Promoting Antigen Cross-Presentation. *Journal of Immunology*, *204*(3): 622-631. https://doi.org/10.4049/jimmunol.1900278

Wei, L., Lin, J. Wu, G. Xu, W. Li, H. Hong, Z., & Peng, J. (2013). *Scutellaria barbata* D. Don induces G1/S arrest via modulation of p53 and Akt pathways in human colon carcinoma cells. *Oncology Reports*, *29*(4): 1623-1628. https://doi.org/10.3892/or.2013.2250

Xu, J., Yu, Y. Shi, R. Xie, G. Zhu, Y. Wu, G., & Qin, M. (2018). Organ-Specific Metabolic Shifts of Flavonoids in *Scutellaria baicalensis* at Different Growth and Development Stages. *Molecules*, *23*(2): 428. https://doi.org/10.3390/molecules23020428

Yang, A. Y., Liu, H. L., & Yang, Y. F. (2022). Study on the mechanism of action of *Scutellaria barbata* on hepatocellular carcinoma based on network pharmacology and bioinformatics. *Frontiers in Pharmacology*, *13*: 1072547. https://doi.org/10.3389/fphar.2022.1072547

Yang, C., Song, J. Hwang, S. Choi, J. Song, G., & Lim, W. (2021). Apigenin enhances apoptosis induction by 5-fluorouracil through regulation of thymidylate synthase in colorectal cancer cells. *Redox Biology*, *47*: 102144. https://doi.org/10.1016/j.redox.2021.102144

Yang, J., Li, Q. Zhou, X. D. Kolosov, V. P., & Perelman, J. M. (2011). Naringenin attenuates mucous hypersecretion by modulating reactive oxygen species production and inhibiting NF-κB activity via EGFR-PI3K-Akt/ERK MAPKinase signaling in human airway epithelial cells. *Molecular and Cellular Biochemistry*, *351*(1-2): 29-40. https://doi.org/10.1007/s11010-010-0708-y

Yang, J. M., Hung, C. M. Fu, C. N. Lee, J. C. Huang, C. H. Yang, M. H. Lin, C. L. Kao, J. Y., & Way, T. D. (2010). Hispidulin sensitizes human ovarian cancer cells to TRAIL-induced apoptosis by AMPK activation leading to Mcl-1 block in translation. *Journal of Agricultural and Food Chemistry*, *58*(18): 10020-10026. https://doi.org/10.1021/jf102304g

Yang, N., Zhao, Y. Wang, Z. Liu, Y., & Zhang, Y. (2017). Scutellarin suppresses growth and causes apoptosis of human colorectal cancer cells by regulating the p53 pathway. *Molecular Medicine Reports*, *15*(2): 929-935. https://doi.org/10.3892/mmr.2016.6081

Yuan, H., Ma, Q. Cui, H. Liu, G. Zhao, X. Li, W., & Piao, G. (2017). How Can Synergism of Traditional Medicines Benefit from Network Pharmacology? *Molecules*, *22*(7): 1135. https://doi.org/10.3390/molecules22071135

Yue, G. G. L., Chan, Y. Y. Liu, W. Gao, S. Wong, C. W. Lee, J. K. M. Lau, K. M., & Lau, C. B. S. (2021). Effectiveness of *Scutellaria barbata* water extract on inhibiting colon tumor growth and metastasis in tumor-bearing mice. *Phytotherapy Research*, *35*(1): 361-373. https://doi.org/10.1002/ptr.6808

Zeng, P., Wang, X. M. Ye, C. Y. Su, H. F., & Tian, Q. (2021). The Main Alkaloids in Uncaria rhynchophylla and Their Anti-Alzheimer's Disease Mechanism Determined by a Network Pharmacology Approach. *International Journal of Molecular Sciences*, *22*(7): 3612. https://doi.org/10.3390/ijms22073612

Zhang, Y., Luo, J. Liu, Z. Liu, X. Ma, Y. Zhang, B. Chen, Y. Li, X. Feng, Z. Yang, N. Feng, D. Wang, L., & Song, X. (2021). Identification of hub genes in colorectal cancer based on weighted gene co-expression network analysis and clinical data from The Cancer Genome Atlas. *Bioscience Reports*, *41*(7): BSR20211280. https://doi.org/10.1042/BSR20211280

Zhang, Z., He, L. Lu, L. Liu, Y. Dong, G. Miao, J., & Luo, P. (2015). Characterization and quantification of the chemical compositions of *Scutellariae barbatae* herba and differentiation from its substitute by combining UHPLC-PDA-QTOF-MS/MS with UHPLC-MS/MS. *Journal of Pharmaceutical and Biomedical Analysis*, *109*: 62-66. https://doi.org/10.1016/j.jpba.2015.02.025

Zheng, R., Zhang, S. Zeng, H. Wang, S. Sun, K. Chen, R. Li, L. Wei, W., & He, J. (2022). Cancer incidence and mortality in China, 2016. *Journal of the National Cancer Center*, *2*(1): 1-9. https://doi.org/10.1016/j.jncc.2022.02.002

Zheng, X., Kang, W. Liu, H., & Guo, S. (2018). Inhibition effects of total flavonoids from *Sculellaria barbata* D. Don on human breast carcinoma bone metastasis via downregulating PTHrP pathway. *International Journal of Molecular Medicine*, *41*(6): 3137-3146. https://doi.org/10.3892/ijmm.2018.3515

Zhou, Y., Zhou, B. Pache, L. Chang, M. Khodabakhshi, A. H. Tanaseichuk, O. Benner, C., & Chanda, S. K. (2019). Metascape provides a biologist-oriented resource for the analysis of systems-level datasets. *Nature Communications*, *10*(1): 1523. https://doi.org/10.1038/s41467-019-09234-6

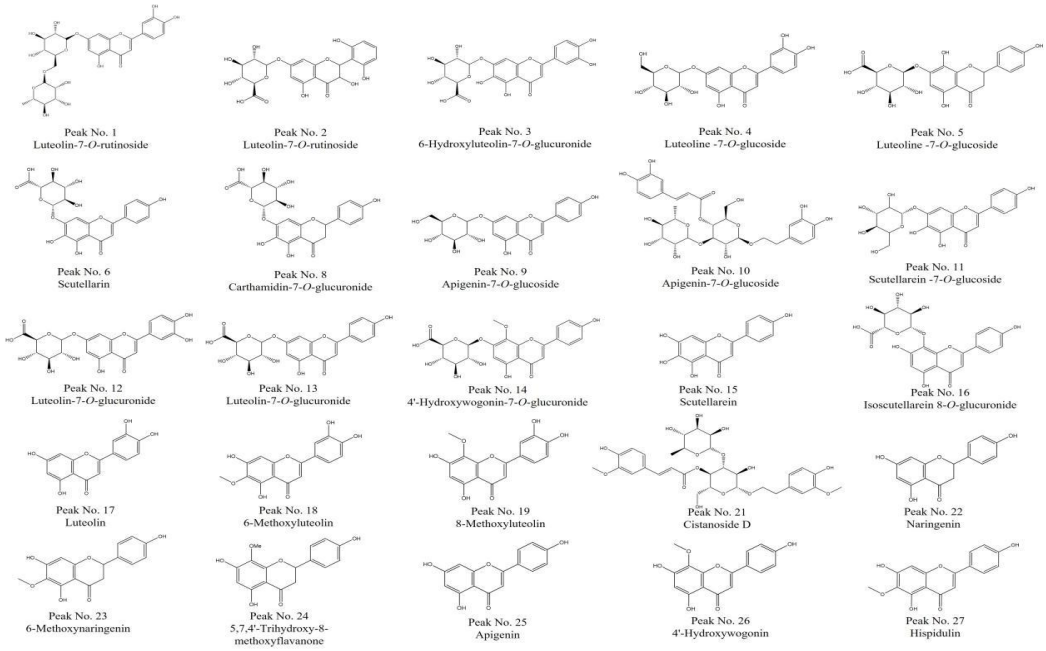

Fig. S1: The structures of the identified compounds in Fig. 2A

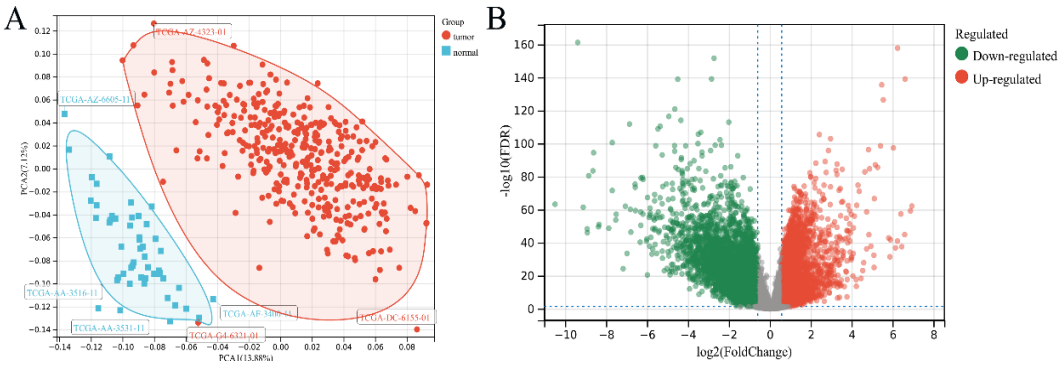

Fig. S2: Identification of DEGs between normal and CRC samples; (A) Principal component analysis of 434 CRC patients; (B) The volcano plot. Green dots represented down-regulated genes, gray dots represent not significant genes and red dots represent up-regulated genes